Delta Channel Networks:

2. Metrics of topologic and dynamic complexity for delta comparison, physical inference and vulnerability assessment

Alejandro Tejedor[1], Anthony Longjas[1], Ilya Zaliapin[3] and Efi Foufoula-Georgiou[1, 2]

[1]National Center for Earth-surface Dynamics and St. Anthony Falls Laboratory, University of Minnesota, Minneapolis, MN, USA 55414

[2]Department of Civil, Environmental and Geo- Engineering, University of Minnesota, Minneapolis, MN, USA 55455

[3]Department of Mathematics and Statistics, University of Nevada, Reno, NV, USA 89557

Water Resources Research

Submitted: October 27, 2014

Revised: March 2, 2015

Abstract

Deltas are landforms that deliver water, sediment and nutrient fluxes from upstream rivers to the deltaic surface and eventually to oceans or inland water bodies via multiple pathways. Despite their importance, quantitative frameworks for their analysis lack behind those available for tributary networks. In a companion paper [*Tejedor et al.*, 2015], we conceptualized delta channel networks as directed graphs and used spectral graph theory to design a quantitative framework for exploring delta connectivity and flux dynamics. Here we use this framework to introduce a suite of graph-theoretic and entropy-based metrics, to quantify two components of a delta's complexity: (1) *Topologic,* imposed by the network connectivity and (2) *Dynamic,* dictated by the flux partitioning and distribution. The metrics are aimed to facilitate comparing, contrasting, and establishing connections between deltaic structure, process, and form. We illustrate the proposed analysis using seven deltas in diverse morphodynamic environments and of various degrees of channel complexity. We project deltas into a topo-dynamic space whose coordinates are given by topologic and dynamic delta complexity metrics, and show that this space provides a basis for delta comparison and physical insight into their dynamic behavior. We also show that the examined metrics relate to the intuitive notion of vulnerability, measured by the impact of upstream flux changes to the shoreline flux, and reveal that complexity and vulnerability are inversely related. Finally, we use a spatially explicit metric, akin to a delta width function, to classify shapes of different delta types.

1. Introduction

Deltas are landforms that deliver sediment, nutrients and water from upstream basins to the shoreline through interconnected pathways of channels. They are highly productive regions with very diverse ecosystems, fertile agriculture areas, and often considerable subsurface resources. As a result, their population density is high with several megacities located in deltas. However, climate (sea level rise) and anthropogenic changes (e.g., upstream dams and local exploration) are putting many deltas in peril [e.g., *Syvitski et al*., 2009; see also *Foufoula-Georgiou et al*., 2013]. Considering that deltas are highly variable in structure, origin and dynamics due to factors such as climate, geology and external forcings, it is important both to identify the bio-physical processes that drive their growth, as well as, understand what perturbations seem to mostly disrupt their functionality and self-maintenance. The question posed in this study is whether we can construct informative metrics of topologic and dynamic complexity of delta channel networks that are rich enough to discriminate between the physical processes that gave rise morphodynamically to these complex networks of drainage paths, as well as, to infer a delta's vulnerability to change. Such metrics are proposed herein and shown to offer significant insights in connecting delta process and form, and in allowing comparison of deltas and inferences about their ability to absorb changes.

The developed metrics rely on a quantitative framework based on spectral graph theory for studying river delta topology and dynamics. The graph-theoretic framework presented in the companion paper [*Tejedor et al*., 2015] allowed us to identify upstream (contributing) and downstream (nourishment) subnetworks for any given delta vertex (node), including the *apex-to-shoreline subnetworks*, referred to also as outlet subnetworks. It also allowed us to compute the steady-state flux propagation in the delta channels and to construct *vulnerability maps* that quantify how a change in any upstream delta link would affect the shoreline fluxes. Based on this analysis, we defined a vulnerability index V_i of an outlet subnetwork S_i draining to the outlet i that quantifies the vulnerability of the outlet flux to local flux changes on all its upstream components. The framework was illustrated in *Tejedor et al*. [2015] using two contrasting deltas: the Wax Lake delta in the coast of Louisiana, USA and the Niger delta in West Africa.

Having established the mathematical machinery based on spectral graph theory that efficiently allows to perform the above computations, we now ask the question as to what quantitative metrics one can build that summarize the topologic complexity of delta networks (reflecting their channel connectivity), as well as their dynamic complexity (reflecting how flux dynamic exchanges happen within the network). Such metrics are absent from the literature hindering further progress in quantifying relations between the morphodynamic processes on the deltaic surfaces and the complex collection of splitting and rejoining channels that these processes imprint on the landscape. *Smart and Moruzzi* [1971], motivated by the exact same problem, presented a preliminary framework based on graph theory by which comparison metrics of delta channel networks could be built. The metric they proposed was a simple one, termed the "recombination factor", and defined as the ratio of the number of junctions (points where two channels combine to form one) to the number of forks (points where one channel divides into two). This recombination

factor was computed for five different deltas and some interesting observations were made. It is unfortunate that not much work (to the best of our knowledge) has followed up since the 1970s along these lines. We see our work as a come-back to this important problem.

A qualitative classification of deltas based on the relative influence of the river, tide and wave effects has been presented by *Galloway* [1975]. A fourth dimension was incorporated into this classification by *Orton and Reading* [1993] to account for the prevailing sediment size delivered to the delta. Some quantitative metrics related to delta morphology have been proposed for river-dominated (minimally affected by waves and tides and bifurcation-dominated) [*Edmonds et al.*, 2011], wave-dominated [*Jerolmack and Swenson*, 2007], and tide-dominated deltas [*Fagherazzi et al.,* 1999; *Rinaldo et al.,* 1999a,b; *Passalacqua et al.,* 2013]. These metrics include fractal properties of the channel network [e.g., *Cleveringa and Oost*, 1999; *Marciano et al.*, 2005; *Seybold et al.*, 2007; *Edmonds et al.*, 2011], non-fractality of shorelines [e.g., *Wolinsky et al.*, 2010], island sizes and their probability distributions [e.g., *Edmonds et al.*, 2011; *Passalacqua et al.,* 2013] but are not directly related to network topology and dynamics. The aim of this paper is to present metrics that we hope will re-open the dialogue started by *Smart and Moruzzi* [1971] on connecting physical properties of deltas to their intricate topologic and dynamic structure and, in addition, allow rigorous analysis of how structure and dynamics predisposes a particular delta to be more vulnerable or more robust to external perturbations.

The developments were motivated by some observations made in our first paper [*Tejedor et al.*, 2015]. As illustrated in Figure 1, for the Wax Lake and Niger deltas the apex is connected to the coast via a number of subnetworks, each one delivering fluxes from the apex to one of the shoreline vertices (outlets). These subnetworks can be topologically very simple (a straight path of channels) or very complex (multiple splitting and merging paths); see Figure 1a and 1b for an example which marks such outlet subnetworks. The topologic complexity of each of the subnetworks is embedded within the whole delta channel network topology to result in various degrees of "dependence" among the subnetworks. Namely, two subnetworks that share no channels at all (except the apex vertex) are considered independent, while two subnetworks which advance together until they split farther downstream to empty their fluxes to different outlets are considered dependent. This is illustrated in Figure 1c and 1d where n (number of subnetworks to which a given link belongs to) depicts quantitatively the simplicity of the Wax Lake delta as compared to the Niger delta. Finally, the dynamic interdependence of the subnetworks, measured in terms of their shared fluxes and the fluxes that leak from one subnetwork to another, rather than in terms of shared links, can be minimal or significant and it relates both to the network topology and the flux distribution within the system. For example, the overall flux interaction will depend on whether the shared subnetwork links are close to the apex (wider channels and larger fluxes) or close to the coast (narrower channels and smaller fluxes). This is schematically illustrated in Figure 1e and 1f. This topologic and dynamic complexity of delta networks directly determines how disturbances in an upstream link will propagate downstream and to the coastal outlets. The propagation of this disturbance from upstream links to the shoreline

was quantified in our earlier paper [*Tejedor et al*., 2015] by a common-sense vulnerability metric that depicts the degree to which the flux at the coastal vertices is affected by local flux changes at all upstream links of the subnetworks [see *Tejedor et al*., 2015 Figure 11].

In this paper, we extend this work and build rigorous metrics that quantify the topologic and dynamic complexity of delta networks and relate it to the notion of vulnerability. In the quest to shed physical insight into what these metrics tell us about the morphological dynamic processes and constraints that gave rise to a delta network we apply our metrics to seven diverse deltas which reveal some interesting findings.

The structure of the paper is as follows. Section 2 presents a brief description of the seven examined deltas and summarizes their basic physical characteristics. In Section 3 we develop a suite of metrics that capture the *topologic complexity* of deltas. Specifically, we consider loopiness, structural overlapping and entropy-based topologic complexity. In Section 4, metrics of *dynamic complexity* are developed. These metrics account not only for topology but also for the distribution of the fluxes among channels of a subnetwork or flux leakage from one subnetwork to the others. The metrics of dynamic complexity introduced here are the subnetwork leakage, flux overlapping and entropy-based dynamic complexity. The metric computation and comparison of seven deltas is presented in Section 5. In Section 6, we illustrate how these metrics can be used to uniquely position a delta on a *delta topo-dynamic space* according to its complexity. We also explore the connection of delta complexity to its vulnerability to change in Section 7. Section 8 goes one step further to acknowledge the fact that the topologic and dynamic complexity of a delta network varies downstream from the apex to the shoreline and attempts to introduce spatially explicit metrics of complexity, leading to the notion of a delta network width function. Overall conclusions and directions for further research are discussed in Section 9.

2. Physical Characteristics of seven deltas analyzed

To aid in the interpretation of the developed complexity metrics we selected a diverse set of delta networks on which these metrics were computed and contrasted. In this section, we summarize the physical characteristics of the seven deltas selected for analysis namely: (1) Niger, (2) Parana, (3) Yukon, (4) Irrawaddy, (5) Colville, (6) Wax Lake and (7) Mossy arranged in order of decreasing size (delta top area). We refer to Figure 2 for the channel networks and Table 1 for physical characteristics of the examined deltas [note that a more detailed account for the Niger and Wax Lake deltas was provided in *Tejedor et al*., 2015].

Extracting the channel networks from an air photo or satellite image of a delta is not an easy task. For this reason we have adopted here for our preliminary analysis the exact five traced deltas in the study of *Smart and Moruzzi* [1971] – Niger, Parana, Yukon, Irrawaddy, and Colville – and have added the Wax Lake and Mossy deltas for which channel networks have been extracted in previous studies [*Edmonds et al.,* 2011]. The issue of what detail one should use in tracing a channel and make it part of the network or ignore it is an important one but not pursued in this study. However, we hope that the metrics presented here will allow the systematic study of the topologic and dynamic complexity of a delta system as a function of the detail at which its network is

abstracted. This issue is further discussed in the conclusions.

Comparison of the set of topologic and dynamic complexities in deltas of different age, size, climate, sediment, external forcing etc. is hoped to provide insight towards the goal of relating physical attributes of the delta generating processes to the complex self-organized arrangement of the channels that nourish and maintain the functionality of the delta system.

Niger Delta: The Niger Delta located in the West coast of Nigeria (latitude 4.95°, longitude 6.18°), receives input from the Niger River at an average water discharge of 6130 m^3 s^{-1} and sediment discharge of 3.97 x 10^7 tons yr^{-1} [*Syvitski et al., 2005*]. The origin of the delta is estimated to be 80 - 35 million years BP during the Late Cretaceous [*Goudie*, 2005]. It is the largest delta in Africa covering an area of 24,508 km^2 and sediment is mostly fine sand [*Orton and Reading,* 1993]. The tidal range is 3.0 m. It is qualitatively classified as tide and wave dominated [*Syvitski et al., 2005*]. We utilized the channel network outlined by *Smart and Moruzzi* [1971], and identified 181 links, 130 vertices and 15 shoreline outlets (see Table 2).

Parana Delta: The Parana Delta, located North of Buenos Aires, Argentina (-33.80°, -59.25°) is fed by the Parana River, which delivers an average water discharge of 13,600 m^3 s^{-1} and sediment discharge of 7.75 x 10^7 tons yr^{-1} [*Syvitski et al., 2005*]. Delta genesis was estimated during the Middle Holocene (6,000 years BP) [*Politis et al.*, 2011]. Parana delta covers an area of 15,463 km^2 and sediment are mostly fine sand, silt and clay [*Fossati et al.*, 2014]. The tidal range is 4.0 m. It is qualitatively classified as a river and geology dominated delta [*Syvitski et al., 2005*]. We utilized the channel network outlined by *Smart and Moruzzi* [1971], and identified 86 links, 69 vertices and 18 shoreline outlets.

Yukon Delta: The Yukon Delta is located in the West coast of Alaska, USA (63.05°, -164.05°) and receives input from the Yukon River with an average water discharge of 6620 m^3 s^{-1} and sediment discharge of 5.97 x 10^7 tons yr^{-1} [*Syvitski et al., 2005*]. Delta genesis is estimated to be during the Middle Holocene (5,000 years BP) [*Nelson and Creager*, 1977]. It has an area covering 8,313 km^2 with mainly fine-grained sediments [*Walker*, 1998]. The tidal range is 1.5 m. It is qualitatively classified as a wave dominated delta [*Syvitski et al., 2005*]. We utilized the channel network outlined by *Smart and Moruzzi* [1971], and identified 169 links, 126 vertices and 24 shoreline outlets in the delta.

Irrawaddy Delta: The Irrawaddy delta, located in the Southernmost coast of Myanmar (16.20°, 95.00°) is fed by the Irrawaddy River at an average water discharge of 13,558 m^3 s^{-1} and sediment discharge of 2.60 x 10^8 tons yr^{-1} [*Syvitski et al., 2005*]. The delta covers an area of 6,438 km^2 with the deposited sediment composed of mostly mixed mud and silt [*Orton and Reading,* 1993]. It is estimated that the delta began to form around 8,000-7,000 years BP together with most of the deltas in Southeast Asia [*Hedley et al.*, 2010]. The tidal range is 4.2 m. It is qualitatively classified as a tide dominated delta [*Syvitski et al., 2005*]. We utilized the channel network outlined by *Smart and Moruzzi* [1971] and identified 100 links, 71 vertices and 6 shoreline outlets in the delta.

Colville Delta: The Colville delta is located in the Northern part of Alaska, USA (70.40°, -150.65°)

and receives input from the Colville River with an average water discharge of 491.7 m^3 s^{-1} [*Orton and Reading,* 1993] and sediment discharge of 1.16 x 10^8 tons yr^{-1} [*Arnborg et al., 1967*]. The delta began to develop during the Middle Holocene (4,000 years BP) [*Jorgenson et al., 1998*]. With an area of 240 km^2, it is relatively small compared to other polar deltas. Sediment is mostly composed of gravel and sand [*Orton and Reading,* 1993]. The tidal range is 0.2 m. It is qualitatively classified as a river dominated delta [*Syvitski et al., 2005*]. We utilized the channel network outlined by *Smart and Moruzzi* [1971], and identified 140 links, 107 vertices and 20 shoreline outlets in the delta.

Wax Lake Delta: The Wax Lake delta is located in the coast of Louisiana, USA (29.51°, -91.44°). It receives input from the Wax Lake outlet, a channel that was dredged in the early 1940s to mitigate flooding risk in the nearby Morgan City, at an average water discharge of 2,900 m^3 s^{-1} and sediment discharge of 2.35 x 10^7 tons yr^{-1} [*Roberts et al.*, 2003]. Sub aerial land only developed after the 1970s flood and has been experiencing rapid growth in the last two decades doubling to more than 100 km^2 today [*Roberts et al.*, 1997; *Paola et al.*, 2011]. Sediment deposit in the delta is composed of approximately 67% sand [*Roberts et al.*, 1997]. The tidal range is 0.40 m [*Shaw et al.*, 203]. It is qualitatively classified as a river dominated delta. We utilized the outline of the Wax Lake delta channel network processed by *Edmonds et al.* [2011] containing 59 links, 56 vertices and 24 shoreline outlets.

Mossy Delta: The Mossy delta is located in Saskatchewan, Canada (54.07°, -102.35°), is fed by the Mossy River with an average water discharge of 300 m^3 s^{-1} [*Edmonds et al., 2011*] and sediment discharge of 2.20 x 10^6 tons yr^{-1} [*Oosterlaan and Meyers*, 1995]. The delta was formed as a result of the avulsion of the Saskatchewan River in the 1870s [*Smith et al.*, 1998]. Progradation of the delta resulted in an area of 14 km^2 in the early 1940s [*Oosterlaan and Meyers*, 1995] and after the construction of a spillway dam in the 1960s, the delta ever since slowly evolved with a current area of approximately 17 km^2. Sediment in the delta is roughly 50% fine-grained sand [*Edmonds et al.*, 2011]. Since the delta drains into a lake (Lake Cumberland), the effect of tides is insignificant. It is qualitatively classified as a river dominated delta. We have extracted the channel network of Mossy delta from a satellite image copyrighted by Digital Globe Inc. 2014 obtained from Google Earth on August 15, 2014 and identified 67 links, 61 vertices and 23 shoreline outlets.

3. Metrics of topologic complexity

As can be visually appreciated in Figure 2, delta channel networks are complex structures with no obvious single attribute that can uniquely describe them. Qualitatively, one can differentiate between mostly bifurcating deltas (Wax Lake and Mossy), deltas that seem to be more constrained throughout their spatial extent (Parana), or constrained mostly close to their apex (Niger, Yukon, Colville), or close to their outlets (Irrawaddy). One can also see that some deltas include more loops than others and that these loops, as well as channel splitting and rejoining, happen at different spatial scales from single channels to tapestries of channels that seem to form sub-deltas within the main delta. Here we attempt to capture these features in a set of quantitative metrics.

For the developments that follow, we need to recall some basic aspects of the graph-theoretic

framework developed in *Tejedor et al*. [2015]. A delta is conceptualized as a directed graph with channels represented by links and junctions by vertices. Link directions correspond to the direction of flux propagation. Hence a delta with N junctions is represented with a directed graph with N vertices. The adjacency matrix A is an $N \times N$ matrix whose element a_{uv} is unity if vertex u receives fluxes directly from vertex v (that is, if vertices u and v are connected by a link directed from v to u) and zero otherwise; see equation (1) and examples in *Tejedor et al*. [2015]. The in-degree (out-degree) matrix D^{in} (D^{out}) is an $N \times N$ diagonal matrix whose elements d_{uu} depict the number of links entering (exiting) vertex u. This matrix D^{in} (D^{out}) is uniquely determined by the adjacency matrix A as its element d_{uu} is the sum of the elements in the *u-th* row (column) of A. Finally, the Laplacian matrix, L^{in} (L^{out}) is defined as D^{in}-A (D^{out}-A). We also recall that the outlet subnetworks are identified by the non-zero elements of the eigenvectors of the matrix $(L^{out})^T$ corresponding to zero eigenvalues [*Tejedor et al*., 2015, Sect. 3.3]. If instead of mere topology we also consider flux propagation, the adjacency matrix A is replaced with the weighted adjacency matrix W, where the weights w_{uv} correspond to the fraction of flux in link (vu) with respect to the flux in vertex v, which can be estimated from channel attributes, such as channel width, depth, and velocity or computed via numerical modeling. In general, a link from vertex v to vertex u is denoted by (vu), and, according to the above nomenclature, it corresponds to the element m_{uv} of the suitable matrix M (adjacency, degree, Laplacian, weight, etc.). We assume that the examined delta has N_o outlets indexed by $i = 1,\ldots, N_o$ and refer to the contributing subnetworks S_i of the i-th outlet as "i-th subnework".

Based on this framework we introduce metrics that are defined here for individual outlet subnetworks, noting that the same metrics can be readily computed for any other non-outlet subnetwork draining to any node of interest different from an outlet node. Specifically, we present a set of six metrics that try to capture three distinctive characteristics of topologic complexity: (1) Loopiness, (2) Structural Overlapping and (3) Entropy-based topologic complexity (see Table 3).

3.1. Subnetwork Loopiness

From inspection of Figure 2, one of the first observations is that young deltas like Mossy or Wax Lake look almost like inverted tributary networks. However, other deltas like Niger or Parana are very far from that approximation since they contain loops at all scales. We introduce two metrics to depict this loopiness characteristic: Number of alternative paths and Resistance Distance.

3.1.1. Number of alternative paths (N_{ap})

This metric corresponds to the intuitive notion of counting how many different ways (called alternative paths, N_{ap}) a package of flux can take to travel from the apex to a given outlet. Thus every fork (bifurcation) in the subnetwork doubles the N_{ap} (recall that in an outlet subnetwork all paths have to converge to a single outlet, so for each fork we necessarily have a stream junction). Note that if there are no junctions, as in the case of a binary tree, then each subnetwork consists of a unique path from the apex to its outlet and such a delta has the minimum Number of alternative paths ($N_{ap} = 1$) for each subnetwork.

Within the graph-theoretic framework [*Tejedor et al*., 2015], it can be shown that the Number of alternative paths, from vertex k to the outlet of

subnetwork S_i, is computed as the k-th component of the eigenvector i of the matrix (I^*-A^T), where A^T is the transpose of the adjacency matrix of the deltaic network, and I^* is obtained from the identity matrix by placing zero in the position (uu) for each outlet u (see Appendix A for proof).

3.1.2. Resistance Distance (*RD*)

Resistance distance is a more sophisticated metric, borrowed from the theory of electrical circuits, which can be used to measure the loopines of a graph. It differs from the Number of alternative paths in the sense that it does not just compute all the possible paths (in a combinatorics sense). The idea behind resistance distance is to compute how well-connected two vertices are in a graph, not just in the sense of how many different paths are in-between them, but also by acknowledging the existence of disjoint paths, i.e., paths that do not contain the same links.

Klein and Randic [1993] defined formally the *Resistance Distance* (*RD*) between two vertices u and v in a graph G as the effective resistance between the two vertices established in an electric circuit network with each link replaced by a 1-ohm resistor. The *RD* is computed using standard series and parallel relations (see Appendix B). Thus, two vertices connected by several paths (parallel connection) have lesser *RD* than if they are connected by only one path (series connection). For example, if there is only one possible path between two vertices, the *RD* is equivalent to the topologic distance (measured in terms of the number of links between the two vertices). We normalize the Resistance Distance between the apex and the subnetwork outlet by the shortest topologic distance between the apex and the outlet. This normalization ensures that the *RD* between any two vertices is within the interval [0,1]. To see this, recall that for a single-path subnetwork the *RD* is equal to the topologic distance, and if we have more than a single path, the *RD* decreases. For a binary tree, the *RD* of every subnetwork is equal to 1. The *RD* is defined for undirected graphs in *Klein and Randic* [1993], so for directed graphs such as delta networks we need to symmetrize the adjacency matrix in computing *RD*. The computation of the *RD* for subnetwork i is done in the following steps:

1. Select the vertices that do not belong to the subnetwork i and redefine the adjacency matrix A by zeroing the columns and rows that correspond to these vertices;
2. Symmetrize the modified Adjacency Matrix: $A_s = (A+A')/2$;
3. Compute the Laplacian L^{out} of the symmetric adjacency matrix A_s;
4. Compute the Moore-Penrose pseudoinverse Γ of the Laplacian [*Penrose*, 1955];
5. The Resistance Distance, $RD(uv)$, between vertices u and v is:
$$RD(uv) = \Gamma_{uu} + \Gamma_{vv} - \Gamma_{uv} - \Gamma_{vu}$$
6. We define the Resistance Distance of the subnetwork i, RD_i, as $RD(uv)$, where v is the apex and u is the outlet of the subnetwork, normalized by the shortest topologic distance between the apex and the outlet.

3.2. Structural Overlapping of Subnetworks

Figure 3 shows some of the outlet subnetworks of Mossy and Parana deltas. The reader can observe how in the Parana delta, many channels belong simultaneously to many subnetworks (black links correspond to the shared links among subnetworks 2-18). On the other hand, Mossy delta only has this kind of overlapping for links located at the top of the structure (black links correspond to the shared links among subnetworks 12, 13 and 18). It

is important to notice that this structural overlapping seems to be a characteristic that varies from delta to delta but also there can be heterogeneity even within a given delta. Thus, in the Mossy delta, some subnetworks can share a lot of links but it is also possible to find subnetworks that are almost independent of each other (e.g., subnetworks 12 and 19). In order to capture all of these conceptual differences we introduce two metrics: Link Sharing Index and Subnetwork to Subnetwork Topologic Pairwise Dependence.

3.2.1. Link Sharing Index (*LSI*)

This metric aims to quantify the overlapping of a subnetwork S_i with other subnetworks in the delta S_j ($j \neq i$). Thus, S_i has a high *LSI* if its links are shared with many other subnetworks in the delta, and low *LSI* if S_i consists of links that are exclusive to it or shared with a very few other subnetworks. For that purpose, we define b_{uv} as the number of subnetworks the link (vu) belongs to. We define the subnetwork Link Sharing Index (*LSI*) by averaging the reciprocal of b_{uv} over all N_i links of S_i:

$$LSI_i = 1 - \frac{1}{N_i} \sum_{(vu)\in S_i} b_{uv}^{-1} . \qquad (1)$$

The index takes values within the interval [0,1) and equals zero if and only if none of the links that form S_i is shared with other subnetworks. For a perfect binary delta of depth d (the number of binary bifurcations from the apex to the outlets), with all outlet vertices having the same depth and a single path from the apex, we have

$$LSI_i = 1 - \frac{1}{d} \sum_{n=1}^{d} \frac{1}{2^{n-1}} = 1 - \frac{2^d - 1}{d 2^{d-1}} . \qquad (2)$$

For d = 2, 5, and 100 we have LSI_i = 0.25, 0.61, and 0.98 for each subnetwork of the perfect binary delta. This metric is useful to distinguish deltas that consist of a set of quasi-independent subnetworks from deltas that contain a substantial "core" common to almost all subnetworks (e.g., see the Parana delta). Note that the variability of *LSI* among subnetworks of a delta system is itself also a metric of topologic complexity, since systems with larger variability of *LSI* values imply more heterogeneous link-sharing structure within the system.

3.2.2. Subnetwork to Subnetwork Topologic Pairwise Dependence (*TPD*)

In order to gain more insight into the subnetwork structural overlapping, which is a measure of the internal heterogeneity of the entire network structure, we define the Subnetwork to Subnetwork Topologic Pairwise Dependence. This metric shows the overlapping for all pairs of subnetworks, offering a picture of the local interaction (in the sense of link sharing) of subnetworks, and therefore with the potential of depicting subunits at mesoscales, which consist of groups of subnetworks. Thus, its value for the pair of subnetworks S_i and S_j is computed as the average of the reciprocal of b_{uv}^{ij} ($b_{uv}^{ij} = 2$ if the link (vu) belongs to both S_i and S_j and $b_{uv}^{ij} = 1$ if it belongs to S_i but not S_j):

$$TPD_{ij} = \frac{1}{N_i} \sum_{(vu)\in S_i} \left(b_{uv}^{ij} \right)^{-1} , \qquad (3)$$

where N_i is the number of links in subnetwork S_i. Notice the asymmetry in the Topological Pairwise Dependence with respect to the indices i and j (i.e., $TPD_{ij} \neq TPD_{ji}$).

3.3. Entropy-based topologic complexity of subnetworks

Historically, entropy was defined as a measure of *disorder*. This interpretation has been widely used in physics and engineering based on the idea that a system evolves into an increasing state of disorder (the second law of thermodynamics); it can also be related to Boltzmann's entropy in statistical mechanics based on the number of microstates [*Prigogine,* 1967; *Boltzmann*, 1872]. *Shannon* [1948] developed an application of entropy to information theory, which is different from the historical idea of disorder and deals with the information that can be gained from the uncertainty in the occurrence of an event. Here we use Shannon's entropy to measure the information content of channel splitting and rejoining in a delta. We note that the information-based entropy has been extensively used in diverse fields ranging from the original application in signal processing [*Shannon,* 1948], to ecology [*Rutledge et al.*, 1976; *Ulanowicz*, 2001], hydrology [*Amorocho and Espildora*, 1973; *Fiorentino et al.*, 1993; *Singh*, 1997 and references therein], ecohydrology [*Ruddell and Kumar*, 2009a,b], and geomorphology [*Leopold and Langbein*, 1962; *Culling*, 1988], among others.

As discussed in *Tejedor et al*. [2015], we adopt a "package of flux" point of view to describe delta flux transport. Namely, we consider a conceptual individual package of flux that enters the system at the apex and propagates downstream until it arrives at a channel junction. Here it randomly decides which of possible further paths to take, with the probability of taking a particular path depending on the channel width or any other suitable characteristic. In other words, the package performs a random directed walk along the network of delta channels. A flow in the delta is conceptualized by a large number of non-interacting flux packages that independently perform such a random downstream walk. To ensure that this process has a well defined steady-state we assume that after reaching an outlet, each package reappears in the apex.

Defining a "state" of this process as the occurrence of a random package at a particular vertex, then p_i is the probability that state i occurs. We can define $(-\log p_i)$ as a measure of the "surprise" that the occurrence of the state i (arrival of package at vertex i) causes. Thus, if $p_i = 1$ (certain event) the surprise is zero and if $p_i = 0$ (impossible event), the surprise is infinity; the surprise grows exponentially from zero to infinity.

The product of the probability of occurrence p_i and the surprisal $(-\log p_i)$ gives us a measure of uncertainty h_i:

$$h_i = -p_i \log p_i . \qquad (4)$$

Therefore, a state that is certain or impossible does not have any uncertainty (i.e., if $p_i = 1$ or 0, $h_i = 0$). Note that h_i is a positive function of p_i in the interval (0,1). We can define the total uncertainty in a system as the sum of the uncertainties of each state:

$$H = \sum_i^N h_i = -\sum_i^N p_i \log p_i . \qquad (5)$$

Notice that the maximum of H is observed when the probabilities of occurrence for all the states are equal.

During the evolution of a system, transitions among states occur as a flux package travels from one vertex to another. If p_{ij} is the probability of

transition from state $j = 1,\ldots,N$ to state $i = 1,\ldots,N$, we can define the uncertainties of those transitions as

$$H = \sum_{i,j}^{N} h_{ij} = -\sum_{i,j}^{N} p_{ij} \log p_{ij} . \qquad (6)$$

For transitions, H is called joint entropy and it can be decomposed into two components: Mutual Information and Conditional Entropy.

Mutual Information (*MI*) is a measure of the amount of information that one state contains about another state (i.e., the reduction of uncertainty in one state due to the knowledge of the other) [*Cover and Thomas*, 2006]. It is expressed as

$$MI = \sum_{i,j}^{N} p_{ij} \log \frac{p_{ij}}{p_i p_j} . \qquad (7)$$

Conditional Entropy (*CE*) is defined as the remaining uncertainty of the state i when j is known and is given by:

$$CE = -\sum_{i,j}^{N} p_{ij} \log p_{j \to i} , \qquad (8)$$

where $p_{j \to i}$ is the probability of transition from j to i given that the initial state is j.

The topologic complexity quantifies the branching and rejoining of channels and not how the flux is distributed. Therefore, to compute the topologic entropy-based metrics we set the probability of splitting in each fork $p_{j \to i}$ as the inverse of the number of offspring vertices. The p_{ij} corresponds to the steady state probability of each transition and can be computed in a similar way as the steady flux calculation in section 3.2 of *Tejedor et al*. [2015] wherein the weighted adjacency matrix W is substituted by the adjacency matrix A. As will be discussed in section 4.3, in considering delta fluxes, the probabilities p_{ij} and $p_{j \to i}$ are computed in terms of the actual partition of fluxes.

4. Metrics of dynamic complexity

In the previous section, we have introduced a set of metrics to quantify the topologic complexity of deltaic networks. However, there is another component of complexity that has not been considered in that analysis, i.e., the complexity introduced by the flux partition in the system. In Figure 4, we present a caricature of two systems with the same underlying network structure and therefore the same basic constraint on the flux partition imposed by their topology. However, their different geomorphologic characteristics may result in a different distribution of fluxes as shown in Figure 4. The necessity of defining a second component of complexity that quantifies the effects of the variability of flux partition in the system is apparent. We denote this component as the dynamic complexity and we argue that together the topologic and dynamic complexities provide a comprehensive, and as we show later non-redundant way of characterizing a delta system. For this, we first develop the dynamic complexity metrics and then we implement both metrics in the seven selected deltas for interpretation and comparison.

The set of metrics to assess the dynamic complexity capture three main characteristics: (1) Leakage, (2) Flux Overlapping and, (3) Entropy-based dynamic complexity (see Table 3). The dynamic computations are based on the values of the steady state flux in each vertex and link of the

examined delta; those can be easily obtained according to the methodology in *Tejedor et al*. [2015] Sect. 3.2. We used here the channel widths as a surrogate for the flux partition [see for example *Bolla Pittaluga et al.,* 2003; *Edmonds et al.,* 2011] although other parameterizations can be used as deemed appropriate for a given delta.

4.1. Subnetwork Leakage

From the point of view of the flux, subnetworks are in general *open* systems, i.e., not all the flux that enters the subnetwork from the apex ends at its outlet, in fact, subnetworks *leak out* flux to the rest of the system. This leaking occurs at the border of the subnetwork, and more specifically at bifurcations wherein one of the downstream channels still belongs to a given subnetwork, but the flux diverted to the other channel eventually drains to a different outlet (i.e., such a link belongs to a different subnetwork). Quantifying the ratio of fluxes leaked by a subnetwork is a surrogate of the "interaction among subnetworks", and thereby, an important characteristic of their dynamic complexity.

Thus, we define the Leakage Index (LI_i) of the outlet subnetwork S_i as the proportion of flux that leaks to other subnetworks with respect to the total steady flux of the subnetwork S_i, where the leakage of flux is computed as the difference between the total vertex flux and total link flux in the subnetwork:

$$LI_i = \frac{\sum_{v \in S_i} F_v - \sum_{(vu) \in S_i} F_{uv}}{\sum_{v \in S_i} F_v}. \qquad (9)$$

Here F_v represents the steady flux at vertex v, F_{uv} the steady flux at link (vu). Note that the flux F_v at the upstream vertex v is equal to or larger than the link flux F_{uv} allowing for possible multiple channels leaving vertex v, $F_{uv} \le F_v$. Similarly, the flux at the downstream vertex u is equal to or larger than F_{uv} allowing for other upstream channels to deliver their flux to vertex u, $F_{uv} \le F_u$.

As mentioned before, we can interpret this measure as the capacity of the subnetworks to *interact* among each other. Thus, an almost "sealed" subnetwork (*LI* close to zero) is able to retain almost all of its flux, having almost no exposure/interaction with other subnetworks. This situation can happen in two extreme and opposite configurations: (1) almost independent subnetworks, where only the apex is shared, or (2) almost completely overlapping subnetworks, where each subnetwork spans the whole system, only differing from each other in their outlets. On the contrary, high *LI* implies that the subnetwork has a large interface of interaction with other subnetworks, and exchanges a significant proportion of its flux. Note that in a binary delta $LI = 0.5$ for all its subnetworks if the partition of fluxes in each bifurcation is equal.

4.2. Flux Overlapping of Subnetworks

In the same way that the structural overlapping has been defined in section 3.2, we define here its dynamic counterpart. Figure 3 shows how a given channel can belong to different subnetworks, and therefore, the steady flux contained in that link will be also shared among those subnetworks. However, there is a crucial difference between these two shared components: from the topologic point of view, the shared links belong equally to all the subnetworks, but from the dynamic point of view, the shared flux can drain preferentially to only one subnetwork. Using the same line of argument as in section 3.2, we present two metrics to capture the different properties of flux

overlapping: Flux Sharing Index and Subnetwork to Subnetwork Dynamic Pairwise Dependence.

4.2.1. Flux Sharing Index (*FSI*)

The goal of this metric is to quantify the degree of flux sharing imposed by the structural overlapping. We define the Flux Sharing Index (FSI_i) for the subnetwork S_i as follows:

$$FSI_i = 1 - \frac{1}{N_i} \sum_{v \in S_i} \gamma_i(v), \qquad (10)$$

where N_i is the number of vertices in the subnetwork S_i and $\gamma_i(v)$ is the proportion of the flux in vertex v that arrives at outlet i (note that $1 - \gamma_i(v)$ is the proportion of flux in vertex v that arrives to any outlet j, $j \neq i$). With this metric, we try to capture the dynamic dependence among the outlet subnetworks. If a subnetwork is totally independent, then $\gamma_i(v) = 1 \ \forall v$ and all of the flux contained in the subnetwork will eventually be delivered to the outlet i. This situation corresponds to $FSI_i \approx 0$. On the other hand, if the subnetwork consists of vertices whose fluxes are shared with many other subnetworks then $\gamma_i(v) \approx 0$ and only a small proportion of the flux in the subnetwork i will be delivered to the outlet. This corresponds to $FSI_i \approx 1$. Recall that $\gamma_i(v)$ can easily be computed as the v-th component of the eigenvector of the matrix $\left(L_W^{\text{out}}\right)^T$ that corresponds to the subnetwork i, and N_i is the number of non-zero components of γ_i [see *Tejedor et al*., 2015].

4.2.2. Subnetwork to Subnetwork Dynamic Pairwise Dependence (*DPD*)

Similar to its topologic counterpart, we look for a deeper understanding of the heterogeneity of the flux distribution within the whole system by examining the flux sharing between subnetworks S_i and S_j. This metric is computed as the ratio of the flux contained in the links that belong to both subnetworks S_i and S_j to the flux contained in the subnetwork S_i:

$$DPD_{ij} = \frac{\sum_{u \in S_{ij}} F(u)}{\sum_{v \in S_i} F(v)}, \qquad (11)$$

where S_{ij} is the set of links that belong to both S_i and S_j, i.e., $S_{ij} = S_i \cap S_j$. Note that if the Topologic Pairwise Dependence between subnetworks S_i and S_j is zero ($TPD_{ij} = 0$), DPD_{ij} is also zero. However, if TPD_{ij} has a high value, it does not guarantee a high value for DPD_{ij} since the flux can travel preferentially to one subnetwork.

4.3. Entropy-based dynamic complexity of subnetworks

Here we develop the entropy concept presented in section 3.3, to incorporate the partition of fluxes. Consider a steady flux $F=(F_1,\ldots,F_N)$ at the vertices of a delta with a weighted adjacency matrix $W=\{w_{uv}\}$ whose element w_{uv} specifies the proportion of the parental flux F_v that goes to its offspring u. We set the stationary probability that the package of flux is travelling from vertex v to vertex u proportional to the flux F_{uv} at the link that connects these vertices:

$$p_{uv} = \frac{F_{uv}}{F^i}, \qquad (12)$$

where $F^i = \sum_{(vu) \in S_i} F_{uv}$ is the total flux in the links of subnetwork S_i. We can now find the probability $p_{\bullet v}$ of a flux package leaving vertex v (while staying

within the subnetwork S_i) proportional to the flux leaving vertex v:

$$p_{\bullet v} = \frac{F_{\bullet v}}{F^i} = \frac{\sum_{u \in S_i} w_{uv} F_v}{F^i} \quad . \qquad (13)$$

Similarly, the probability $p_{u\bullet}$ of a flux package arriving at vertex u from subnetwork S_i is proportional to the flux entering u:

$$p_{u\bullet} = \frac{F_{u\bullet}}{F^i} = \frac{\sum_{v \in S_i} w_{uv} F_v}{F^i} \, . \qquad (14)$$

Recall that the joint entropy of a discrete distribution $\{p_{uv}\}$ as defined in section 3.3, equation (6) can be computed as:

$$H = -\sum_{(vu) \in S_i} p_{uv} \log p_{uv} \, . \qquad (15)$$

The joint entropy can be partitioned into two components: Mutual Information and Conditional Entropy. The Mutual Information (*MI*), defined in equation (7) as a measure of the amount of information shared by the pairs of vertex u and v, can be expressed in terms of the flux partition w_{uv} as:

$$MI = \sum_{(vu) \in S_i} p_{uv} \log \frac{p_{uv}}{p_{u\bullet} p_{\bullet v}} = \sum_{(vu) \in S_i} p_{uv} \log \frac{w_{uv}}{p_{\bullet v}} \, . \qquad (16)$$

The Conditional Entropy (*CE*) defined in equation (8) as the average uncertainty that remains about v when u is known can be expressed as:

$$CE = -\sum_{(vu) \in S_i} p_{uv} \log \frac{p_{uv}^2}{p_{u\bullet} p_{\bullet v}} \, . \qquad (17)$$

The entropy can be interpreted as the ability of the system to undergo changes [*Ulanowicz et al.*, 2009] or in other words, it quantifies how the uncertainty of the system enables it to deal with perturbations. Notice that for subnetworks consisting of linear paths, *CE*=0 since $p_{uv} = p_{u\bullet} = p_{\bullet v}$, therefore for a binary delta the *CE* is zero for all its subnetworks.

5. Metric computation and comparison of seven deltas

5.1. Loopiness and Leakage of subnetworks

From simple inspection of Figure 2, we can differentiate two major groups of deltas: (1) bifurcation-dominated (e.g., Wax Lake and Mossy) and (2) loop-dominated (e.g., Niger, Yukon, Irrawaddy, Parana, and Colville). The metrics of loopiness that we have presented are able to capture this separation: bifurcation-dominated deltas are characterized by a low Number of alternative paths (N_{ap}) and a high Resistance Distance (*RD*) (see Figure 5a and Figure 6a). In bifurcation-dominated deltas, most of the subnetworks do not have alternative paths; in fact, single paths connecting the delta apex to the shoreline outlets comprise 75% (18/24) and 70% (16/23) of the subnetworks for the Wax Lake and Mossy deltas, respectively, and this is translated to *RD* equal to 1. On the other hand, in loop-dominated deltas all of the subnetworks have multiple paths connecting the apex to the outlet, having values of *RD* significantly lower than 1 (medians are in the interval 0.6 – 0.83). More information can be untangled with a detailed comparison of those two metrics. First, the N_{ap} of Yukon stands out with respect to the other deltas. However, the range of values of *RD* for Yukon is comparable with other deltas like Niger and Colville. This is revealing the fact that the loopines in Yukon is happening at a smaller scale

(loops consisting of fewer links) than in the other deltas, increasing drastically the N_{ap} but not reducing so much the equivalent *RD*. Besides, the fact that the number of paths in Yukon is high for almost all the subnetworks reveals that those small-scale loopy structures are close to the apex. On the other hand, there are deltas like Parana and Irrawaddy that have intermediate values for the N_{ap}, and relatively low values of *RD*. This tendency reveals the existence of complicated structures at small and medium scales. The higher *RD* of Parana is the result of its particular structure, wherein the upper part is clearly loop-dominated, but in its lower region, its structure changes to bifurcation-dominated, increasing the values of *RD* (see Figure 2). Figure 6b highlights the potential of N_{ap} and *RD* to extract complementary information of loopiness since they do not trivially relate to each other across deltas (i.e., different slopes for different deltas).

We have characterized the topologic complexity of the subnetworks (apex to outlet) in terms of their loopines. However this difference in their topology can lead to more profound consequences in their dynamic interaction. We have defined the Leakage Index (*LI*) to quantify those interactions as it measures the flux exchange among subnetworks. Thus, we can observe that subnetworks with high topologic complexity (in terms of loopiness) normally have lower *LI*. However, that relation is not trivial, since even though the underlying topology is a major constraint in the distribution of the steady flux, the process-specific dynamic partition of flux plays an important role. Deltas with similar loopiness, in terms of median and variability among subnetworks, such as Irrawaddy and Parana, can have subnetwork leakage that significantly differs (in fact, reverses) in variability. On the other hand, deltas as different as Niger and Wax Lake in terms of median and variability of their loopiness have similar median, although vastly different variability, for their subnetwork leakage (see Figure 5b).

Recall here that the Leakage Index measures the proportion of the flux that leaves a given subnetwork. Notice that those losses only take place in the junctions that form the border of the subnetwork; we refer to those junctions as *external*. Thus, subnetworks that contain a low ratio of internal to external junctions will be more prone to leaking out flux and therefore have high values of *LI*, and vice versa. Subnetworks with a high value of loopiness are more likely to have a high value of the internal to external junction ratio, in agreement with previous results shown in this section. It is also important to notice at this point, that *LI* is also sensitive to the flux partition, so the presence of preferential paths for flux can change substantially the value of *LI* for a given topology. Therefore it is understandable how deltas with similar topologies, such as Irrawaddy and Parana, can have quite different *LI*.

5.2. Structural and flux overlapping of subnetworks

We have argued in sections 3 and 4 how the overlapping in topology and flux among subnetworks is an important factor in assessing the complexity of the entire delta network. To measure the degree to which a subnetwork shares its channels and fluxes with other subnetworks, we have introduced the Link Sharing Index (*LSI*) and Flux Sharing Index (*FSI*). Figure 5c1 and 5c2 show that both *LSI* and *FSI* have the same general trend in their medians but *FSI* has a larger variability for all deltas. This is expected since there is no possible dynamic sharing (fluxes)

without topologic sharing (channels). Therefore, the flux sharing can be interpreted as a modulation of the link sharing. Thus, differences between the dynamic and topologic sharing tell us about the asymmetry in the flux distribution. If we examine this closer, we note that Yukon and Parana have high *LSI* implying the existence of a core of links that are common to several subnetworks. For Yukon, the range of variability of *FSI* is similar to the range of variability for *LSI*, suggesting an almost equitable distribution of fluxes among the different subnetworks. On the contrary, for deltas such as Irrawaddy and Niger the ranges of variability of *FSI* are much bigger than those for *LSI*, indicating a more asymmetric distribution of fluxes (presence of preferential pathways of flux delivery to the shoreline). In other words, for Parana and Yukon deltas (high values for *LSI* and *FSI*) there is not only topologic overlapping (links shared by subnetworks) but also dynamic overlapping wherein flux in each link is also shared by other subnetworks. On the other hand, for Irrawaddy and Niger deltas, links are relatively equally-shared among subnetworks but the dynamic components are preferentially shared in a sense that a large percentage of the flux in a given link drains to one subnetwork relative to the others (common topologic units but more independent dynamic units).

The metrics discussed above can be useful in characterizing the overall topologic and dynamic dependence of each subnetwork. However, understanding the nature of those relationships (e.g., subnetworks that overlap with a few or a large number of other subnetworks) is necessary in order to tease apart the complexity of the delta as a whole. Thus, we present a joint representation that captures those relationships, namely: Subnetwork to Subnetwork Topologic and Dynamic Pairwise Dependence.

Figure 7 shows for three deltas (Mossy, Niger and Parana) the results of the pairwise analysis of topologic (left panels) and dynamic (center panels) dependence. Here the outlets are indexed consecutively and counterclockwise starting with the leftmost one where the delta is plotted with the apex on the figure's top and outlets at the bottom. From the topologic pairwise analysis, tree-like deltas (e.g., Mossy) exhibit high values of shared links (red colors) close to the diagonal, and low otherwise. This means that only neighboring subnetworks have a significant number of common links, which decreases fast when compared to farther subnetworks. Deltas like Niger present a similar diagonal-pattern in the topologic pairwise analysis. At the same time, the dynamic counterpart is clearly different between these two delta types. Specifically, in the analysis of bifurcation-dominated deltas, some structures appear symmetrically along the diagonal, meaning that for many pairs (i,j) subnetwork i shares the same proportion of flux with j as j shares with i. However, for loop-dominated deltas the Dynamic Pairwise Dependence is not symmetric at all. The contiguous areas of high values of sharing in both charts can be interpreted as mesoscale units in the delta, consisting of several subnetworks (see Figure 7 right panels), that emerge from either the topologic or their dynamic overlapping (or both). Thus, in tree-dominated deltas, the subnetworks separate from each other close to the apex and do not rejoin again, hence forming different topologic units. Although, the flux is subject to the constraint imposed by the mentioned topology, red colors (high pairwise dependence) are also observed for subnetworks located away from each other in the dynamic chart of Mossy delta. This is

due to the fact that, although far away subnetworks only share a few channels, those channels are located close to the apex and can contain a big percentage of the total flux. On the other hand, in more complex deltas e.g., those that have experienced major avulsions, due to the existence of loops close to the apex, both topologic and dynamic interactions among farther subnetworks are present. Parana exhibits a paradigm of extensive systemwise interaction, where the system acts almost as a single unit; this is also reflected in the very small variability among the 18 outlet subnetworks in all the computed metrics (see Figure 5).

5.3. Entropy-based complexity of subnetworks

Entropy measures the complexity in terms of the uncertainty in the splitting and rejoining paths (topologic) and fluxes (dynamic). Traditionally, joint entropy is divided into two components the Mutual Information (*MI*) and Conditional Entropy (*CE*). A noteworthy insight is the interpretation of *MI* and *CE* as measures of *Rigidity* and *Flexibility*, respectively for both network topology and dynamics; see also *Ulanowicz et al.* [2009]. We relate the concept of *MI* with rigidity, interpreted as a measure of the constraints imposed by the connectivity of the channel networks. Recall that *MI* measures the information shared between states, and in deltas those possible connections require a physical connectivity (channel network). On the other hand, *CE* is a measure of the remaining information contained in the system once the structure is imposed. The source of that remaining information is the uncertainty still present in the system about the next position (state) of a package of flux given the knowledge of its current position. Thus, subnetworks consisting of single paths have zero *CE,* since no further information is gained when the structure is fixed (i.e., given the current position of the package of flux, we know that its next position is directly downstream of the current one). Subnetworks with at least one bifurcation have non-zero *CE* since even though the structure is known, the voyage of the package of flux is not totally determined (i.e., in each bifurcation, there is some uncertainty related to the probability of taking one or other alternative path).

From the computation of these metrics, Figure 5d1 and 5d2 show similar trends and variability for both the topologic and dynamic Mutual Information (*MI*) revealing that connectivity is the most important constraint underlying this concept of complexity. The fact that measures of loopiness, N_{ap} and *RD*, exhibit similar trends and variability to those of *MI* reinforces its interpretation as the Rigidity of the system.

The trend and variability seen for the topologic and dynamic *MI* is not generally observed for Conditional Entropy (see Figure 5e1, and 5e2): (i) the dynamic *CE* is smaller than the topologic *CE*, (ii) big changes in the variability of those two magnitudes are observed for the same delta (e.g., higher topologic than dynamic variability for Niger and lower topologic than dynamic variability for Irrawaddy), and (iii) same trends and variability are observed for bifurcation-dominated deltas such as Wax Lake and Mossy. These differences and similarities can be interpreted in terms of the flexibility of the system: (i) since flexibility deals with the information that remains in the system because of the uncertainty introduced in each bifurcation, its maximum value occurs when there is equal probability of splitting. This implies that topologic *CE* is always greater than or equal to the dynamic *CE*; (ii) Flexibility is very sensitive to flux partition. Therefore, having symmetric or asymmetric partition in each fork

generates different variability across subnetworks for topologic and dynamic *CE*; (iii) the similarity in the topologic and dynamic *CE* for Wax Lake and Mossy deltas resides in their bifurcation-dominated nature wherein very little further information is gained since most of the subnetworks are single paths (*CE* =0).

6. Constructing a Topo-Dynamic Complexity Space for Deltas

Having developed the framework to assess the complexity of deltas, it is now possible to push forward the idea of defining a complexity space where deltas can be mapped and compared. Different topologic and dynamic characteristics of a delta can be considered coordinates of a *Topo-Dynamic* complexity space. A particular choice of the examined characteristics (and hence space dimension) would depend on the specific problem being addressed. For illustration purposes we have chosen two metrics, one topologic and one dynamic, to construct a topo-dynamic space for the seven examined deltas. We have chosen the Number of alternative paths (N_{ap}) as a surrogate for Topologic Complexity and the Leakage Index (*LI*) for Dynamic Complexity. The resulting space is shown in Figure 8, which shows the median and interquartile range (the range between 25% and 75%) for each space component and every delta. A general trend is observed: the more topologically complex a delta is, the lower its dynamic complexity although the variability of each component (coming from the collection of subnetworks in each delta) can be very large. This trend is expected since the larger the topologic complexity, the smaller the proportion of external links (border), which are able to interact with the rest of the delta, and therefore the lesser the possibility of fluxes leaking out. The special case of a binary tree delta (with equal flux partition in each bifurcation) has the minimum topologic complexity (N_{ap}=1), i.e., all the subnetworks consist of a linear path, and a dynamic complexity *LI* = 0.5, as illustrated in Figure 8. We observe that the Wax Lake and Mossy deltas are the closest to that binary tree, depicting the almost bifurcating topology but also the more complex dynamics due to flux sharing. In spite of this general trend, other interesting and more detailed properties can also be observed. For example, deltas like Colville and Yukon have similar dynamic complexity, but Yukon is clearly more complex in terms of topology. Likewise, Colville and Niger have comparable topologic complexity, but Niger is more dynamically complex. A more detailed explanation of the meaning of those similarities and differences has been presented in the previous sections, together with other metrics, but what we attempt to put forward here is the idea of a simple representation, in which both the topologic and dynamic complexity are able to position deltas in a common space to quantitatively compare and eventually classify them.

7. Relating the concepts of Complexity and Vulnerability

In *Tejedor et al.* [2015], vulnerability was defined in terms of how changes in upstream links would affect the shoreline fluxes. We now ask the question of whether and how the vulnerability of the system might relate to its complexity. We illustrate in Figure 9 the comparison between the average Vulnerability Index V_i for the different delta subnetworks as defined in *Tejedor et al.* [2015] equation (14) and (a) the topologic complexity and (b) dynamic complexity. We have chosen the Number of alternative paths (N_{ap}) as a surrogate for topologic complexity and the Conditional Entropy (*CE*) for dynamic

complexity. As expected, the higher the Number of alternative paths, the lower the vulnerability index but the relation is not trivial (Figure 9a). Note that in the vulnerability analysis, single path subnetworks are the most vulnerable since a change of flux in that path propagates directly to the outlet. At the same time, subnetworks with multiple splitting and joining paths are less vulnerable. However, the degree of vulnerability depends on the specific topology of the subnetwork as indicated by the variability associated with the values for individual subnetworks. We also observe the appearance of "unoccupied areas" in this space: there are no subnetworks with high (low) Number of alternative paths and high (low) vulnerability.

From Figure 9b we observe that the Vulnerability Index has a however general decreasing trend with the dynamic *CE*, although the scatter around this relationship is more pronounced compared to that between the Vulnerability and the Number of alternative paths (Fig. 9a). The observation that there are no low (high) values of the vulnerability index when the dynamic *CE* is low (high), reinforces the inverse relationship between vulnerability and complexity. We have chosen the weighted *CE* as a surrogate for dynamic complexity since it can be interpreted as the flexibility of the subnetworks to deliver fluxes to the outlets. Note that the vulnerability index cannot be uniquely determined by either the topologic or the dynamic complexity separately, revealing the necessity of a multivariate analysis and reinforcing the need for a quantitative framework using both the topologic and dynamic complexities to better understand vulnerability. The exact relationship between vulnerability and the topo-dynamic complexity is of course complicated. A 3D space that considers these three quantities jointly would be revealing but it is left for future research.

8. Spatially explicit metrics of complexity: a delta width function

All the metrics developed so far study subnetworks as units without reference to their complexity at specific distances from the apex. It is of interest however to examine how this complexity might change as one moves downstream from the apex to the shoreline. As a preliminary step in this direction we introduce here the *delta width function*, defined as the number of links intersected at different distances from the apex, similar to the width function for river networks defined as the number of streams at a given distance from the outlet [*Rodriguez-Iturbe and Rinaldo*, 1997]. Figure 10 (right panels) illustrates this concept where for simplicity distance is measured radially from the apex. Normalizing this distance by the maximum distance (distance from apex to the actual shoreline) and normalizing the number of links at a given distance by the maximum possible number of links intercepted at any distance, Figure 10a shows the normalized width function for the seven deltas. Also for comparison, the normalized width function of a binary bifurcating tree is displayed on the same plot (notice that its staircase shape is due to the strict hierarchy of the tree together with the assumption of equal link lengths at each level of generation). We observe that for tree-like deltas (Wax Lake and Mossy), the normalized number of links is an increasing function of the normalized distance achieving the maximum at the current shoreline similar to the behavior for the binary tree. More complex deltas, on the other hand, attain a maximum before the current shoreline (e.g., Irrawaddy at normalized distance ≈ 0.78, Colville and Niger ≈ 0.90, and Yukon ≈

0.95) except for Parana with maximum located at the current shoreline. These results highlight the idea that Parana can be thought of as two deltas in tandem [*Smart and Moruzzi,* 1971]: the upper half near the apex with a narrow region similar to braided rivers containing the core links, and the lower half with a topology similar to a bifurcation-dominated delta.

The width function is a useful tool to differentiate among different configurations of delta networks. Figure 11 illustrates schematically the different trends of the width function and their interpretations. An increasing trend for a range of distances from the apex is associated with *divergent* structures, i.e., dominated by bifurcations. On the other hand, a decreasing trend is indicative of *convergent* structures, i.e., confluence-dominated area of the delta. Finally, if a region has a similar number of confluences and bifurcations, it is indicative of a *confined* structure and will manifest itself as a constant width function. According to this classification, tree-dominated deltas such as Mossy and Wax Lake are characterized by mostly divergent structures. Loop-dominated deltas exhibit a convergent structure for a range of distances close to the shoreline. Lastly, the Parana delta is a clear example of a delta with a confined structure where the width function is fairly constant over a large part of the delta (normalized distance of 0.2 to 0.8 from the apex to the outlet; see Figure 10a).

Although the spatial analysis of a mature delta cannot be used as a surrogate for its temporal evolution (due to the possibility of internal rearrangement of channels caused by avulsions and major flooding) it can still be used as a rough proxy. Figure 10b shows the evolution of the seven deltas in the topo-dynamic space. The arrows indicate the direction of increasing distance from the apex. Each line corresponds to the mean topologic complexity and to the mean dynamic complexity as we move from the apex to the shoreline. From a spatial evolution perspective, deltas evolve by increasing their topologic complexity (in terms of N_{ap}) and decreasing their dynamic complexity (in terms of *LI*). This is compatible with the idea that young (old) deltas are topologically simple (complex) with subnetworks exchanging a large (small) proportion of fluxes.

9. Conclusions and open problems

In *Tejedor et al.* [2015], we introduced a framework based on spectral graph theory, by which delta channel networks can be studied as rooted directed acyclic graphs opening the door to efficiently compute several properties of interest via simple algebraic manipulations. Specifically, we demonstrated how upstream (contributing) and downstream (nourishment) subnetworks can be identified and extracted by operations on the so-called Adjacency matrix, which uniquely characterizes the connectivity of a graph. Approaching propagation of fluxes via a random walk on a network, steady-state solutions of fluxes were obtained via the Laplacian operator (similar to the known advection-diffusion operations on a porous medium). The present paper builds on the results of spectral graph theory to define a number of metrics that depict the topologic and dynamic complexity of delta channel networks, a necessary step in the quest of understanding how the physical processes forming a delta relate to the complex transport pathways they leave behind on the landscape. The topologic complexity metrics we proposed depict three topologic characteristics: Loopiness, Structural Overlapping and Entropy-based topologic complexity, while the dynamic

complexity metrics are grouped to capture three main dynamic features: Leakage, Flux Overlapping and Entropy-based dynamic complexity. We used entropy concepts to quantify how the flux between links, constrained by the organized patterns of splitting and re-joining, partitions the total entropy into Mutual Information (rigidity) and Conditional Entropy (flexibility). Finally, we introduced the delta width function that can be used to classify deltas according to their spatially-explicit network configuration. All metrics were implemented and compared on seven diverse deltas.

The results have provided some valuable insights with main conclusions being:

(1) Jointly, the topologic and dynamic complexity of a river delta places it in a unique position in a *delta topo-dynamic space*, revealing that as topologic complexity decreases (e.g., fewer loops and simpler subnetwork structures connecting the apex to the shoreline outlets) the dynamic complexity (flux exchanged among subnetworks) increases. At the limit of minimum (maximum) topologic (dynamic) complexity is a purely bifurcating tree and we see that the simpler and younger (e.g., Mossy and Wax Lake) deltas are, in fact, closer to such a bifurcating delta in the topo-dynamic space. This is also observed in all other metrics.

(2) A spatially-explicit interrogation of a delta in terms of its normalized number of links versus normalized distance from the apex (*delta width function*) reveals that one can quantify easily deltas that are mostly divergent, convergent or geologically confined, as well as transitions from one regime to another. This is apparent in the mostly bifurcating (divergent) structure of the Wax Lake and Mossy deltas, and depicts the mostly confined structure of the Parana delta.

(3) A *tapestry* plot that records the topologic (link sharing between subnetworks) and dynamic (flux sharing between subnetworks) structure of a delta as a whole system, can be used to identify coherent subunits of a delta and provide a complementary representation of its spatial topologic and dynamic structure.

(4) The topologic and dynamic complexity of deltas seem to relate to its vulnerability to change, i.e., to the way a delta responds in propagating upstream disturbances to its shoreline outlets. Specifically, we report an inverse non-trivial relationship between vulnerability and two indices of topologic (Number of alternative paths) and dynamic (Conditional Entropy) metrics.

This study is seen as the beginning of further exploratory analysis of deltas to understand and quantify how bio-physical processes, climate and geologic constraints, as well as human actions, change the topologic and dynamic connectivity of deltaic surfaces and thus affect the way deltas will respond to future perturbations. Two ideas for future work are proposed herein:

(1) Although considerable satellite imagery for deltas is available, automatic extraction of delta channels from such images is not possible hampering extensive analysis not only of a much larger number of deltas, but also a single delta under different seasonal flows or as it has evolved over time. An interesting question to address will be to examine how the scale at which a delta is seen (detail of mapping its channels) affects the metrics of topologic and dynamic complexity and what scale is necessary to achieve some robustness on these metrics. Are there any scaling relationships (akin to those in tributary channel

networks and also in braided river networks, e.g., see *Sapozhnikov and Foufoula-Georgiou,* 1997) that can relate properties of the system at one scale to those at another scale? Is there scale-invariance present in any of those relationships? For example, do smaller in size subnetworks leak out more flux in a way that can be parameterized by size and complexity?

(2) In addition to the natural observatories of deltas, where analysis is based on real data, numerical observatories which can provide a wealth of simulated deltas under controlled physical conditions are expected to provide considerable insight on the problem of how physical processes building a deltaic surface express themselves in the spatial and temporal patterns of its channel structures. For example, numerical simulations based on detailed hydrodynamic models have shown that the shape and the structure of deltas depend on the cohesiveness of the soil [*Caldwell and Edmonds,* 2014], forcings such as wind waves and tides [*Nardin and Fagherazzi*, 2012; *Leonardi et al.*, 2013] etc. Also reduced complexity models [*Liang et al.,* 2015a,b] offer a simpler way to experiment with semi-physical rules and map their effect on the delta channel structure. Such models also offer a mechanism for studying the question as to how the complexity of a single delta evolves over time as the delta builds and its channels avulse due to localized instabilities, propagating laterally and downstream and reorganizing portions of the deltaic surface.

Appendix A: Finding the Number of Alternative Paths to an Outlet

Here we show how to compute the number of alternative paths from a given node within a delta to any given outlet using simple matrix operations on the directed graph G that describes the delta. Two paths are considered different if they differ by at least one non-shared link.

Number of alternative paths: *Consider a delta system represented by an acyclic rooted directed graph G with adjacency matrix A. Assume that the system has k outlets indexed as i =1,…,k. Consider the matrix* $M = (I^*\text{-}A^T)$*, where* A^T *is the transpose of the adjacency matrix, and I* is obtained from the identity matrix by placing zero in the position (uu) for each outlet u. Then*

(i) *The null space of M has dimension (multiplicity of the eigenvalue zero) equal to the number of outlets k;*

(ii) *There exists a unique basis* γ_i*, i=1,…,k, of this null space in* $\mathbb{R}^N$ *(*i.e., *the basis consists of k vectors each having N components) with the property*

$$\gamma_i(j) = \delta_{ij} = \begin{cases} 1, & i = j; \\ 0, & i \neq j \end{cases} \qquad \text{for } j=1,\ldots k.$$

That is, the component of the vector γ_i *is unity at the outlet i (*$\gamma_i(i)=1$*) and zero at all other outlets (*$\gamma_i(j)=0$ *for* $j \neq i$*, j=1,…,k).*

(iii) *The non-outlet vertex v belongs to the contributing subnetwork* S_i *if and only if* $\gamma_i(v) \neq 0$.

(iv) *The value* $\gamma_i(v)$ *equals the number of alternative paths from vertex v to the outlet i.*

Proof:

(i) We observe that there exists at least one indexing of the vertices of the rooted directed acyclic graph G such that each offspring vertex has a higher index than its parental vertex. In this indexing, the internal vertices have indexes from 1 to (|V| - k) -- |V| being the number of the vertices in G -- and the outlets have indexes from (|V| - k

+1) to |V|. By construction, the matrix M is upper triangular, with ones on the main diagonal for the first (|V| - k) rows and with the last k rows being zero. Using the rank-nullity theorem [*Meyer,* 2000], dim($ker(M)$) = k.

(ii) Consider an eigenvector γ that corresponds to the eigenvalue 0 of the matrix $M=(I^*-A^T)$. By the definition of the eigenvalue

$$(I^*-A^T)\ \gamma = I^*\gamma - A^T\gamma = 0, \qquad (1)$$

which implies

$$I^*\gamma = A^T\ \gamma. \qquad (2)$$

In coordinate form, this becomes

$$\gamma(v) = \sum_j a_{jv}\gamma(j) \quad \textit{(for v that are not outlets.)} \ (3)$$

In other words, $\gamma(v)$ is the sum of the components $\gamma(u_i)$ of all the offspring $\{u_i\}$ of v within G.

Next, we explicitly construct k independent eigenvectors that correspond to the zero eigenvalue of M. Namely, the i-th eigenvector γ_i will correspond to the outlet i = 1,…,k. It is constructed by letting $\gamma_i(i) = 1$ and $\gamma_i(j) = 0$ for all the other outlets (that is for all j =1,…,k such that $j \neq i$) and computing the other components using Eq. (3). The linear independence of the vectors $\{\gamma_i\}$ follows from the above construction of the components for the outlet indices: only one vector has non-zero value at coordinate i = 1,…,k. The characteristic property *(ii)* holds by construction.

The above procedure produces k independent vectors. Since the dimension of the kernel of M is k, we constructed a basis for this kernel.

(iii) Follows from construction of the vector components using Eq. (3), as described in the proof of *(ii)* above.

(iv) We prove the statement by induction. The induction base is given by the observation that $\gamma_i(i) = 1$ for the outlet i of the subnetwork S_i, which can be interpreted as the existence of a unique path from the outlet to itself. For induction step we consider an interval vertex v and assume that for all its offspring u_j the number of alternate paths from u_j to the outlet i is given by $\gamma_i(u_j)$. We have

$$\gamma_i(v) = a_{u_1v}\gamma_i(u_1) + ... + a_{u_kv}\gamma_i(u_k) = \gamma_i(u_1) + ... + \gamma_i(u_k),$$

which is indeed the number of paths from v to i. This completes the proof.

Remark: We notice that the above result is very similar to our statements on finding contributing and nourishing subnetworks in the companion paper [*Tejedor et al.,* 2015]. However, this result, unlike those in [*Tejedor et al.*, 2015], does not follow from the work of *Caughman and Veerman* [2006], since it involves the matrix M that cannot be represented as $D(I-S)$, with D being a non-negative diagonal and S – stochastic.

Appendix B: Resistance Distance

A schematic representation of two subnetworks is shown in Figure A1: Subnetwork 1 (top) connecting the Apex to the Outlet 1 (O1), and Subnetwork 2 (bottom) joining the Apex to Outlet 2 (O2). Both subnetworks have the same number of links equal to 6 and the shortest path from the apex to the outlet consisting of 3 links. Here, we want to introduce with more detail concepts related with Resistance Distance (*RD*) described in section 3.1.2, and show differences in the way it quantifies the complexity of a subnetwork with respect to the Number of alternative paths (N_{ap}). Following *Klein and Randic* [1993], we can define Resistance Distance between the apex and the

outlet, as the effective resistance between them when each link of the graph is replaced by a 1-ohm resistor. In the theory of electrical circuits, the effective resistance is computed based on the arrangement of the resistors:

(1) *Resistors in series*: The connected resistors only share one junction (black square), so the current flows through one resistor after the other (e.g., Resistors 1-2-3 and 4-5-6, see top panel of Figure A1). The effective resistance of resistors in series is equal to the sum of the values of the individual resistors,

$$R_{Series} = \sum R_i \quad \text{(A1)}$$

(2) *Resistors in parallel*: The connected resistors share two junctions, so the current flows at the same time to both resistors (e.g., Resistors 1 and 4, 2 and 5, 3 and 4; see bottom panel of Figure A1). The effective resistance of resistors in parallel can be computed as:

$$R_{Parallel} = \left(\sum \frac{1}{R_i} \right)^{-1} \quad \text{(A2)}$$

Therefore, the equivalent resistance from Apex to Outlet 1 and Outlet 2 are as follows:

$$R_{A,O1} = \left(\frac{1}{3} + \frac{1}{3} \right)^{-1} = 1.5$$

$$R_{A,O2} = \left(\frac{1}{1} + \frac{1}{1} \right)^{-1} + \left(\frac{1}{1} + \frac{1}{1} \right)^{-1} + \left(\frac{1}{1} + \frac{1}{1} \right)^{-1} = 1.5$$

Note that both subnetworks have the same Resistance Distance. Resistance Distance can be interpreted as the "effective distance", in the sense that if multiple routes connect two vertices of a graph, these vertices are *closer* to each other than if they are connected only by one route. Thus, the apex is three links apart from both outlets 1 and 2, but the Resistance Distance is half of that number implying the existence of alternative routes between them. On the other hand, the Number of alternative paths between the apex and outlet O1 is 2 (Paths: 1-2-3, and 4-5-6) while the Number of alternative paths between the apex and outlet O2 is 2^3=8 (Paths: 1-2-3, 1-2-6, 1-5-3, 1-5-6, 4-2-3, 4-2-6, 4-5-3 and 4-5-6).

Both metrics can be used to characterize the complexity of the topologic structure, but they are not equivalent. While the Number of alternative paths is able to account for all the possible combinations of paths, Resistance Distance looks at the alternative routes; penalizing some combinations that do not really add *disjoint* paths.

Acknowledgement. This paper precipitated from discussions at the STRESS 4 (Stochastic Transport and Emergent Scaling on the Earth's surface) working group meeting at Lake Tahoe, Nevada on April 2013. This work is part of the International BF-DELTAS project on "*Catalyzing action towards sustainability of deltaic systems*" funded by the Belmont Forum (NSF grant EAR- 1342944). It is also a tribute to the "Sustainable Deltas 2015" (SD2015) Initiative endorsed by the International Council of Scientific Unions (ICSU), which aims to increase awareness of delta vulnerability worldwide and foster international collaboration, knowledge and data exchange for actionable research towards delta sustainability. Partial support by the FESD Delta Dynamics Collaboratory (NSF grant EAR-1135427) and the Water Sustainability and Climate Program (NSF grant EAR- 1209402) is gratefully acknowledged. The data in our article can be provided upon request (alej.tejedor@gmail.com). We would also like to thank the editor Graham Sander, Phairot Chatanantavet and two anonymous reviewers for their helpful comments that resulted in an improved presentation of our work.

Notations

A	*adjacency matrix*
A_s	*symmetrized adjacency matrix*
a_{uv}	*element of A*
b_{uv}	*number of subnetworks link (vu) belongs to*
CE_i	*Conditional Entropy in subnetwork i*
d	*depth of the binary tree*
d_{uu}	*elements of the degree matrix D*
DPD_{ij}	*Dynamic Pairwise Dependence between subnetworks i and j*
D^{in}	*in-degree matrix*
D^{out}	*out-degree matrix*
DCE_i	*Dynamic Conditional Entropy in subnetwork i*
DMI_i	*Dynamic Mutual Information in subnetwork i*
F^i	*total flux in the links of subnetwork i*
F_u	*steady flux at vertex u*
F_{uv}	*steady flux at link (vu)*
FSI_i	*Flux Sharing Index of subnetwork i*
h_i	*measure of uncertainty of state i*
H	*total uncertainty*
I^*	*identity matrix with zeros in the elements corresponding to the outlets*
L^{in}	*in-degree directed graph Laplacian*
L^{out}	*out-degree directed graph Laplacian*
L_W^{out}	*weighted out-degree directed graph Laplacian*
LI_i	*Leakage Index in subnetwork i*
LSI_i	*Link Sharing Index among subnetworks i*
MI_i	*Mutual Information in subnetwork i*
n	*number of subnetworks to which a given link belongs to*
N_o	*number of outlets*
N_i	*number of links/vertices in subnetwork i*
$N_{\text{ap},i}$	*Number of alternative paths in subnetwork i*
p_i	*probability that state i occurs*
p_{ij}	*probability of transition from state j to state i*
p_{uv}	*probability that the package of flux is travelling from vertex v to vertex u*
$p_{u\cdot}$	*probability of a package of flux arriving at vertex u*
$p_{\cdot v}$	*probability of a package of flux leaving vertex v*
$p_{j\to i}$	*probability of transition from j to i given that the initial state is j*
RD_i	*Resistance Distance in subnetwork i*
S_i	*subnetwork i*
S_{ij}	*intersection of links/vertices in subnetworks i and j*

TPD_{ij}	*Topologic Pairwise Dependence between subnetworks i and j*
TCE_i	*Topologic Conditional Entropy in subnetwork i*
TMI_i	*Topologic Mutual Information in subnetwork i*
u	*vertex*
V_i	*global vulnerability of outlet subnetwork i*
w_{uv}	*element of W*
W	*weighted adjacency matrix*
$\gamma_i(v)$	*proportion of flux at vertex v that arrives at outlet i*
Γ	*Moore-Penrose pseudoinverse of the Laplacian*

References

Amorocho, J., and B. Espildora (1973), Entropy in the assessment of uncertainty in hydrologic systems and models, *Water Resour. Res.*, 9(6), 1511-1522, doi:10.1029/WR009i006p01511.

Arnborg, L., H. J. Walker, and J. Peippo (1967), Suspended load in the Colville River, Alaska, 1962, *Geografika Ann.*, 49A, 131–144.

Bolla Pittaluga, M., R. Repetto, and M. Tubino (2003), Channel bifurcations in braided rivers: Equilibrium configurations and stability, *Water Resour. Res.*, 39(3), 10-46, doi:10.1029/2001WR001112.

Boltzmann, L., Weirere Studien uber das warmegleich-gewich unter gasmolekulen, *K. Acad. Wiss. (Wein) Sitzb.*, II Abt, p. 66, 1872.

Caldwell, R. L., and D. A. Edmonds (2014), The effects of sediment properties on deltaic processes and morphologies: A numerical modeling study, *J. Geophys. Res. Earth Surf.*, 119, 961–982, doi:10.1002/2013JF002965.

Cleveringa, J., and A. P. Oost (1999), The fractal geometry of tidal-channel systems in the Dutch Wadden Sea, *Geol. en Mijnb*ouw, 78, 21–30.

Cover, T. M., and J. A. Thomas (2006), Elements of Information Theory 2nd ed., 748 pp., John Wiley & Sons Inc., Hoboken, N. J.

Culling, W. E. H. (1988), Dimension and entropy in the soil-covered landscape, *Earth Surf. Proc. Land.*, 13: 619-648. doi: 10.1002/esp.3290130706.

Edmonds, D. A., and R. L. Slingerland (2007), Mechanics of river mouth bar formation: Implications for the morphodynamics of delta distributary networks, *J. Geophys. Res.*, 112, F02034, doi:10.1029/2006JF000574.

Edmonds, D. A., and R. L. Slingerland (2008), Stability of delta distributary networks and their bifurcations, *Water Resour. Res.*, 44, W09426, doi:10.1029/2008WR006992.

Edmonds, D. A., and R. L. Slingerland (2010), Significant effect of sediment cohesion on delta morphology, *Nat. Geosci.*, 3(2), 105-109, doi:10.1038/ngeo730.

Edmonds, D. A., C. Paola, D. C. J. D. Hoyal, and B. A. Sheets (2011), Quantitative metrics that describe river deltas and their channel networks, *J. Geophys. Res.*, 116, F04022, doi:10.1029/2010JF001955.

Fagherazzi, S., A. Bortoluzzi, W. E. Dietrich, A. Adami, S. Lanzoni, M. Marani, and A. Rinaldo (1999), Tidal networks: 1. Automatic network extraction and preliminary scaling features from digital terrain maps, *Water Resour. Res.*, 35(12), 3891-3904, doi:10.1029/1999WR900236.

Fiorentino, M., P. Claps, and V. P. Singh (1993), An entropy-based morphological analysis of river basin networks, *Water Resour. Res.*, 29(4), 1215-1224, doi:10.1029/92WR02332.

Fossati, M., F. Cayocca, and I. Piedra-Cueva (2014), Fine sediment dynamics in the Río de la Plata, *Adv. Geosci.*, 39, 75-80, doi:10.5194/adgeo-39-75-2014.

Foufoula-Georgiou, E., et al. (2013), A vision for a coordinated international effort on delta sustainability, in Deltas: Landforms, Ecosystems and Human Activities, edited by G. Young & G.M.E. Perillo, IAHS Publ. 358, 3-11.

Galloway, W. E. (1975), Process framework for describing the morphologic and stratigraphic evolution of deltaic depositional systems, In *Deltas: Models for Exploration,* ed. ML Broussard, pp. 87–98, Houston Geol. Soc., Houston, Texas.

Goudie, A. S. (2005), The drainage of Africa since the Cretaceous, *Geomorphology*, 67, 437-456.

Hedley, P. J., M. I. Bird, and R.A.J. Robinson (2010), Evolution of the Irrawaddy delta region since 1850, *The Geographical Journal,* 176(2), 138-149, doi: 10.1111/j.1475-4959.2009.00346.x

Jerolmack, D. J., and J. B. Swenson (2007), Scaling relationships and evolution of distributary networks on wave-influenced deltas, *Geophys. Res. Lett.*, 34, L23402, doi:10.1029/2007GL031823.

Jorgenson, M.T., Y. L. Shur, and H. J. Walker (1998), Evolution of a permafrost-dominated landscape on the Colville River Delta, Northern Alaska, PERMAFROST-Seventh International Conference (Proceedings), Yellowknife (Canda), Collection Nordicana No 55.

Klein, D. J., and M. Randic (1993), Resistance Distance, *J. Math. Chem.*, 12, 81-95.

Leonardi, N., A. Canestrelli, T. Sun, and S. Fagherazzi (2013). Effect of tides on mouth bar morphology and hydrodynamics. *J. Geophys. Res. Oceans,* 118, 4169–4183, doi:10.1002/jgrc.20302.

Leopold, L. B., and W. B. Langbein (1962), The concept of entropy in landscape evolution, *U.S. Geol. Surv. Prof. Pap.*, *500-A*, 20 pp.

Liang, M., V. R. Voller, and C. Paola (2015a), A reduced-complexity model for river delta formation: Part 1 – Modeling deltas with channel dynamics, *Earth Surf. Dynam.*, 3, 67-86, doi:10.5194/esurf-3-67-2015, 2015.

Liang, M., N. Geleynse, D. A. Edmonds, and P. Passalacqua (2015b), A reduced-complexity model for river delta formation: Part 2 – Assessment of the flow routing scheme, *Earth Surf. Dynam.*, 3, 87-104, doi:10.5194/esurf-3-87-2015, 2015.

Marciano, R., Z. B. Wang, A. Hibma, H. J. de Vriend, and A. Defina (2005), Modeling of channel patterns in short tidal basins, *J. Geophys. Res.*, 110, F01001, doi:10.1029/2003JF000092.

Meyer, C. D., Matrix Analysis and Applied Linear Algebra, 2nd ed., SIAM, Pennsylvania, 2000.

Nardin, W., and S. Fagherazzi (2012), The effect of wind waves on the development of river mouth bars, *Geophys. Res. Lett.,* 39, L12607, doi:10.1029/2012GL051788.

Nelson, H., and J. S. Creager (1977), Displacement of Yukon derived sediment from Bering Sea to Chukchi Sea during Holocene times, *Geology*, 5, 141-146.

Oosterlaan, S., and M. Meyers, (1995) Evolution of the Mossy delta in relation to hydrodam construction and lake level fluctuation, University of Illinois, Chicago, 31 pp.

Orton, G. J., and H. G. Reading (1993), Variability of deltaic processes in terms of sediment supply, with particular emphasis on grain size, Sedimentology, 40, 475–512, doi:10.1111/j.1365-3091.1993.tb01347.x.

Paola, C., R. R. Twilley, D. A. Edmonds, W. Kim, D. Mohrig, G. Parker, E. Viparelli, and V. R. Voller (2011), Natural Processes in Delta Restoration: Application to the Mississippi Delta, *Annu. Rev. Mar.*

Sci., 3, 67-91, doi: 10.1146/annurev-marine-120709-142856.

Passalacqua, P., S. Lanzoni, C. Paola, and A. Rinaldo (2013), Geomorphic signatures of deltaic processes and vegetation: The Ganges-Brahmaputra-Jamuna case study, *J. Geophys. Res. Earth Surf.*, 118, 1838-1849, doi:10.1002/jgrf.20128.

Penrose, R. (1955), A generalized inverse for matrices, *Proc. Camb. Philos. S.-M.*, 51, 406-413.
Politis, G. G., M. Bonomo, C. Castiñeira, and A. Blasi (2011), Archaeology of the Upper Delta of the Paraná River (Argentina): Mound Construction and Anthropic Landscapes in the Los Tres Cerros locality, *Quatern. Int.*, 245, 74-88.

Prigogine, I., *Introduction to Thermodynamics of Irreversible Processes*, 3rd ed., John Wiley, New York, 1967.

Rinaldo, A., S. Fagherazzi, S. Lanzoni, M. Marani, and W. E. Dietrich (1999a), Tidal networks: 2. Watershed delineation and comparative network morphology, *Water Resour. Res*., 35(12), 3905–3917, doi:10.1029/1999WR900237.

Rinaldo, A., S. Fagherazzi, S. Lanzoni, M. Marani, and W. E. Dietrich (1999b), Tidal networks: 3. Landscape-forming discharges and studies in empirical geomorphic relationships, *Water Resour. Res.*, 35(12), 3919-3929, doi:10.1029/1999WR900238.

Roberts, H. H., N. Walker, R. Cunningham, G. P. Kemp, and S. Majersky (1997), Evolution of sedimentary architecture and surface morphology: Atchafalaya and Wax Lake Deltas, Louisiana (1973-1994), *Gulf Coast Assoc. Geol. Soc. Trans.*, 47(42) 477-484.

Roberts, H. H., J. M. Coleman, S. J. Bentley, and N. Walker (2003), An embryonic major delta lobe: a new generation of delta studies in the Atchafalaya-Wax Lake Delta system, *Trans. Gulf Coast Assoc. Geol. Soc.,* 53 690–703.

Rodriguez-Iturbe, I., and A. Rinaldo (1997), *Fractal River Basins: Chance and Self-Organization*, 547 pp., Cambridge University Press, Cambridge, UK.

Ruddell, B. L., and P. Kumar (2009a), Ecohydrologic process networks: 1. Identification, *Water Resour. Res.*, 45, W03419, doi:10.1029/2008WR007279.

Ruddell, B. L., and P. Kumar (2009b), Ecohydrologic process networks: 2. Analysis and characterization, *Water Resour. Res.*, 45, W03420, doi:10.1029/2008WR007280.

Rutledge, R. W., B. L. Basore, and R. J. Mulholland (1976), Ecological stability: An information theory viewpoint, *J. Theor. Biol.*, 57(2), 355–371, DOI: 10.1016/0022-5193(76)90007-2.

Sapozhnikov, V. B., and E. Foufoula-Georgiou (1997), Experimental evidence of dynamic scaling and indications of self-organized criticality in braided rivers, *Water Resour. Res.*, 33(8), 1983-1991, doi: 10.1029/97WR01233.

Seybold, H., J. S. Andrade Jr., and H. J. Herrmann (2007), Modeling river delta formation, *Proc. Natl. Acad. Sci. U. S. A.*, 104, 16804-16809, doi: 10.1073/pnas.0705265104.

Shannon, C. E. (1948), A mathematical theory of communication, *The Bell System Technical Journal,* 27, 379–423, 623–656.

Shaw, J. B., D. Mohrig, and S. K. Whitman (2013), The morphology and evolution of channels on the Wax Lake Delta, Louisiana, USA, *J. Geophys. Res. Earth Surf.*, 118, 1562-1584, doi:10.1002/jgrf.20123.

Singh, V.P. (1997), The use of entropy in hydrology and water resources, *Hydrol. Process.*, 11, 587-626 doi: 10.1002/(SICI)1099-1085(199705)11:6<587::AID-HYP479>3.0.CO;2-P.

Smart, J. S., and V. L. Moruzzi (1971), Quantitative properties of delta channel networks, Technical Report #3, 27 pp., IBM Thomas J. Watson Research Center, Yorktown Heights, New York.

Smith, N. D., R. L. Slingerland, M. Perez-Arlucea, and G. S. Morozova (1998), The 1870s avulsion of the Saskatchewan River, *Can. J. Earth Sci.*, 35, 453–466, doi:10.1139/e97-113.

Syvitski, J. P. M., A. J. Kettner, A. Correggiari, and B. W. Nelson (2005), Distributary channels and their impact on sediment dispersal, *Mar. Geol.*, 222-223, 75-94.

Syvitski, J. P. M. et al. (2009), Sinking deltas due to human activities, *Nat. Geosci.,* 2(10), 681-686, doi:10.1038/ngeo629.

Tejedor, A., A. Longjas, I. Zaliapin, and E. Foufoula-Georgiou (2015), Delta Channel Networks: 1. A graph-theoretic approach for studying connectivity and steady-state transport on deltaic surfaces, *Water Resour. Res., this issue*.

Ulanowicz, R.E. (2001), Information theory in ecology, *Computers and Chemistry*, 25, 393-399.

Ulanowicz, R. E., S. J. Goerner, B. Lietaer and R. Gomez (2009), Quantifying sustainability: Resilience, efficiency and the return of information theory, *Ecol. Complex.*, 6 27-36.

Walker, H. J. (1998), Arctic Deltas, *J. Coastal Res.,* 14(3), 718-738.

Wolinsky, M. A., D. A. Edmonds, J. Martin, and C. Paola (2010), Delta allometry: Growth laws for river deltas, *Geophys. Res. Lett.*, 37, L21403, doi:10.1029/2010GL044592.

TABLES

Table 1. Location and summary of physical characteristics for each delta.

Delta	Location	Area (km^2)	Age (yrs)	Apex to shoreline average distance (km)	Dominant Forcing	References
1. Niger	Nigeria	24,508	Late Cretaceous[+] (80-35 Million BP)	160	Wave/Tide[*]	[+] *Goudie*, 2005; [*] *Syvitski et al., 2005*
2. Parana	Argentina	15,463	Middle Holocene[+] (6,000 BP)	213	River/Geology[*]	[+] *Politis et al.*, 2011; [*] *Syvitski et al., 2005*
3. Yukon	Alaska, USA	8,313	Middle Holocene[+] (5,000 BP)	80	Wave[*]	[+] *Nelson and Creager*, 1977; [*] *Syvitski et al., 2005*
4. Irrawaddy	Myanmar	6,438	Middle Holocene[+] (8,000-7,000 BP)	117	Tide[*]	[+] *Hedley et al.*, 2010; [*] *Syvitski et al., 2005*
5. Colville	Alaska, USA	240	Middle Holocene[+] (4,000 BP)	22.5	River[*]	[+] *Jorgenson et al., 1998;* [*] *Walker, 1998*
6. Wax Lake	Louisiana, USA	100	75[+]	11.5	River[*]	[+] *Roberts et al.*, 1997; [*] *Edmonds et al., 2011*
7. Mossy	Canada	17	140[+]	4.7	River[*]	[+] *Smith et al.*, 1998; [*] *Edmonds et al., 2011*

Table 2. Summary of simple topologic characteristics of each delta channel network. The recombination factor introduced by *Smart and Moruzzi* [1971] is computed based on rudimentary graph theory. Note that the values reported here for Niger, Parana, Yukon, Irrawaddy and Colville have been obtained from the analysis of the images by *Smart and Moruzzi* [1971]; values for Wax Lake were obtained from the analysis of the network extracted by *Edmonds et al.* [2011]; and values for Mossy were obtained from the analysis of the network extracted from Google Earth.

Delta	**N_L # of links**	**N_V # of vertices**	**N_O # of outlets**	**N_J # of junction vertices**	**N_F # of fork vertices**	**Recombination factor $\alpha=N_J/N_F$**
1. Niger	181	130	15	50	65	0.769
2. Parana	86	69	18	18	33	0.545
3. Yukon	169	126	24	37	65	0.569
4. Irrawaddy	100	71	6	30	35	0.857
5. Colville	140	107	20	34	53	0.642
6. Wax Lake	59	56	24	5	27	0.185
7. Mossy	67	61	23	10	28	0.357

Table 3. Summary of metrics.

Metrics	Description
A. Metrics of Topologic Complexity	
1. Loopiness 1.1. Number of alternative paths 1.2. Resistance Distance	Quantifies the loopiness of each subnetwork via (1.1) the intuitive notion of the Number of alternative paths from the apex to the outlet and (1.2) the notion of equivalent resistance in the theory of electrical circuits.
2. Structural Overlapping 2.1. Link Sharing Index 2.2. Subnetwork to Subnetwork Topologic Pairwise Dependence	Quantifies the degree to which the network links are shared among (2.1) different outlet subnetworks and (2.2) pairs of subnetworks.
3. Entropy-based Topologic Complexity 3.1. Topologic Mutual Information 3.2. Topologic Conditional Entropy	Quantifies the (3.1) rigidity and (3.2) flexibility in the system imposed by the underlying topologic connectivity.
B. Metrics of Dynamic Complexity	
4. Subnetwork Leakage	Leakage Index measures the proportion of flux leaking from a subnetwork before the flux is delivered to the outlet.
5. Flux Overlapping 5.1. Flux Sharing Index 5.2. Subnetwork to Subnetwork Dynamic Pairwise Dependence	Quantifies the degree to which the network fluxes are shared among (5.1) different outlet subnetworks and (5.2) pairs of subnetworks.
6. Entropy-based Dynamic Complexity 6.1. Dynamic Mutual Information 6.2. Dynamic Conditional Entropy	Quantifies the (6.1) rigidity and (6.2) flexibility in the system taking into account physical processes that control the partition of fluxes.

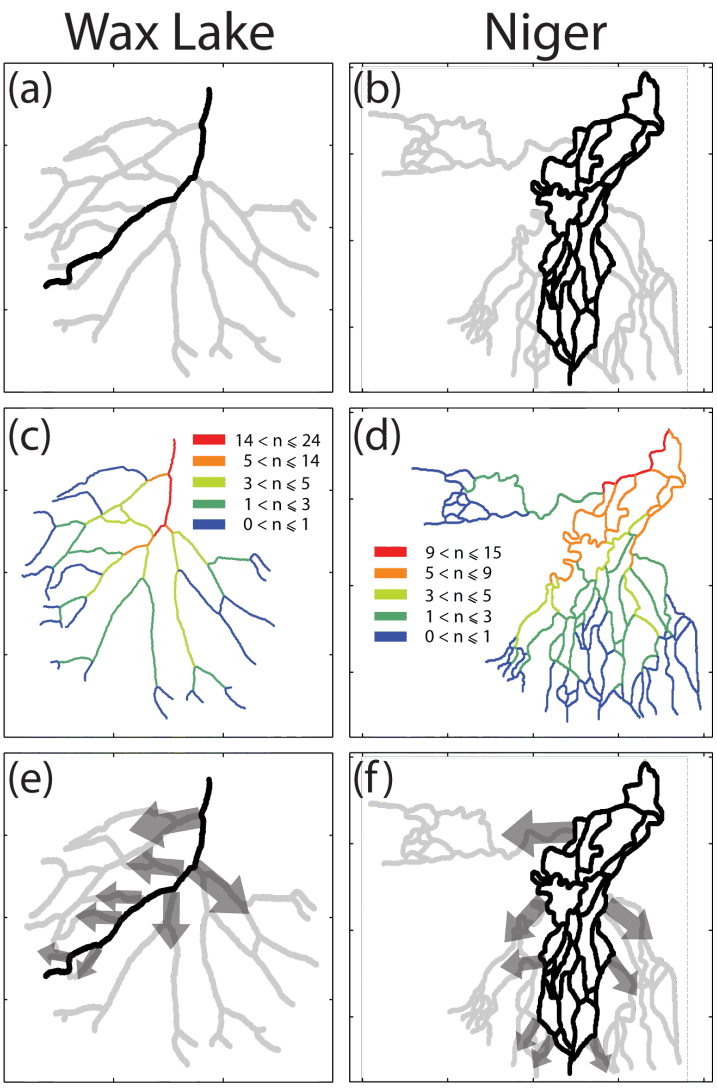

Figure 1. Qualitative illustration of topologic and dynamic complexity of delta channel networks. Panels (a,b): topologic complexity of subnetworks within a delta system ranging from a single path to a collection of splitting and rejoining paths connecting the apex to the outlet. Panels (c,d): shared links among subnetworks that drain to different outlets – a link might be part of only one subnetwork (n=1) or a number of subnetworks n depending on the overall topologic structure of the delta system. Panels (e,f): flux interaction among subnetworks -- bifurcation of channels within a subnetwork that led their fluxes to another subnetwork characterize the dynamic exchange of fluxes and depends both on the topology of the network and also the flux distribution.

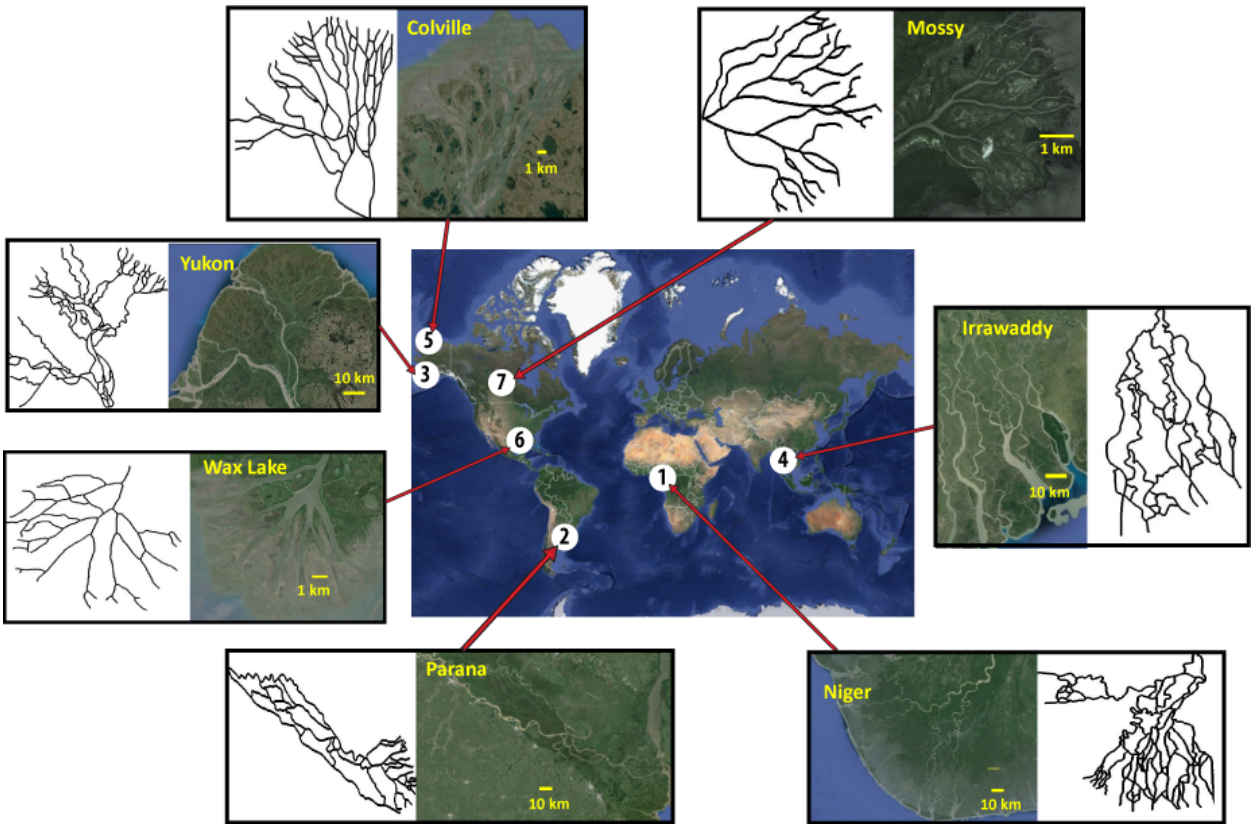

Figure 2. Location of seven deltas and their corresponding channel networks numbered according to size (largest to smallest area). We used the *Smart and Moruzzi* [1971] networks for (1) Niger, (2) Parana, (3) Yukon, (4) Irrawaddy, and (5) Colville Deltas. For (6) Wax Lake we used the network extracted by *Edmonds et al.* [2011]. We have extracted the network of (7) Mossy from Google Earth. Satellite images are copyrighted by Digital Globe Inc. 2014.

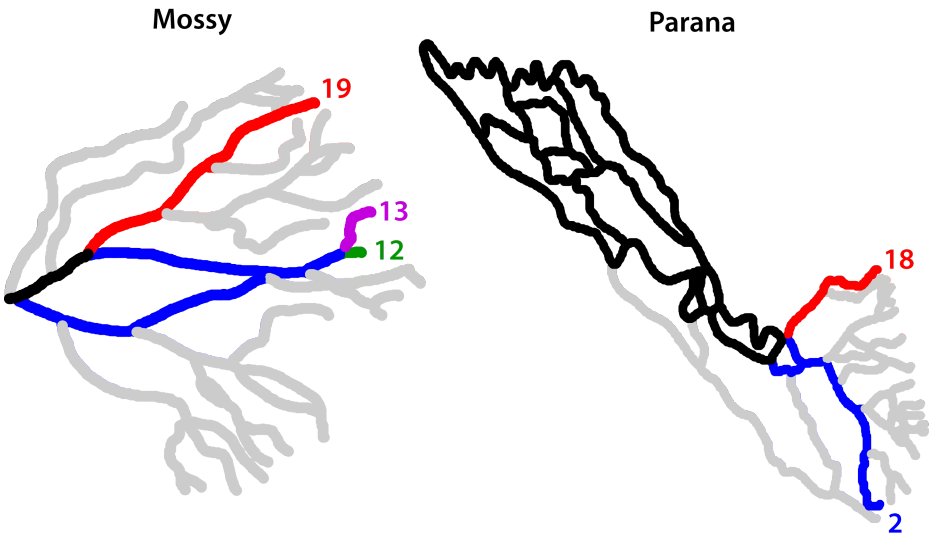

Figure 3. Structural Overlapping. (Left panel) Three different outlet subnetworks have been highlighted for the Mossy delta. Black links represent the common part to the 3 subnetworks, and blue channels the common part to subnetworks 12 and 13, but not to 19. (Right panel) Outlet subnetworks 2 and 18 of Parana delta are highlighted. Black links represent the common part to both subnetworks.

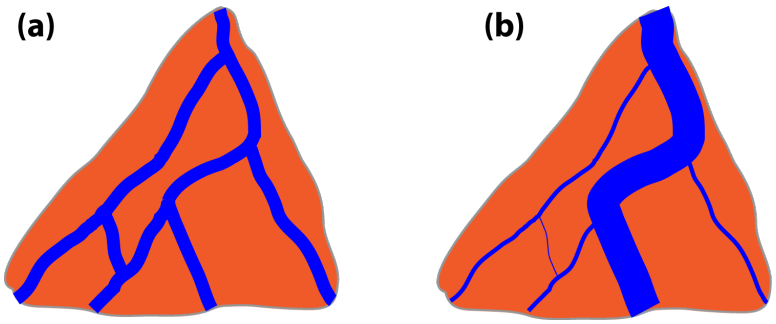

Figure 4. Asymmetric Flux distribution. Caricatures (a) and (b) illustrate two deltas with the same underlying topology (channel network structure) but different flux distribution. The amount of flux in each channel is illustrated by the width of the blue lines. Thus, (a) shows a delta where fluxes are evenly distributed among the different channels, while (b) presents a delta with a clear preferential path by which the main portion of flux is delivered from the apex to the shoreline. As expected, these deltas cannot be differentiated based on their topologic complexity, but only based on their dynamic complexity, which is significantly different.

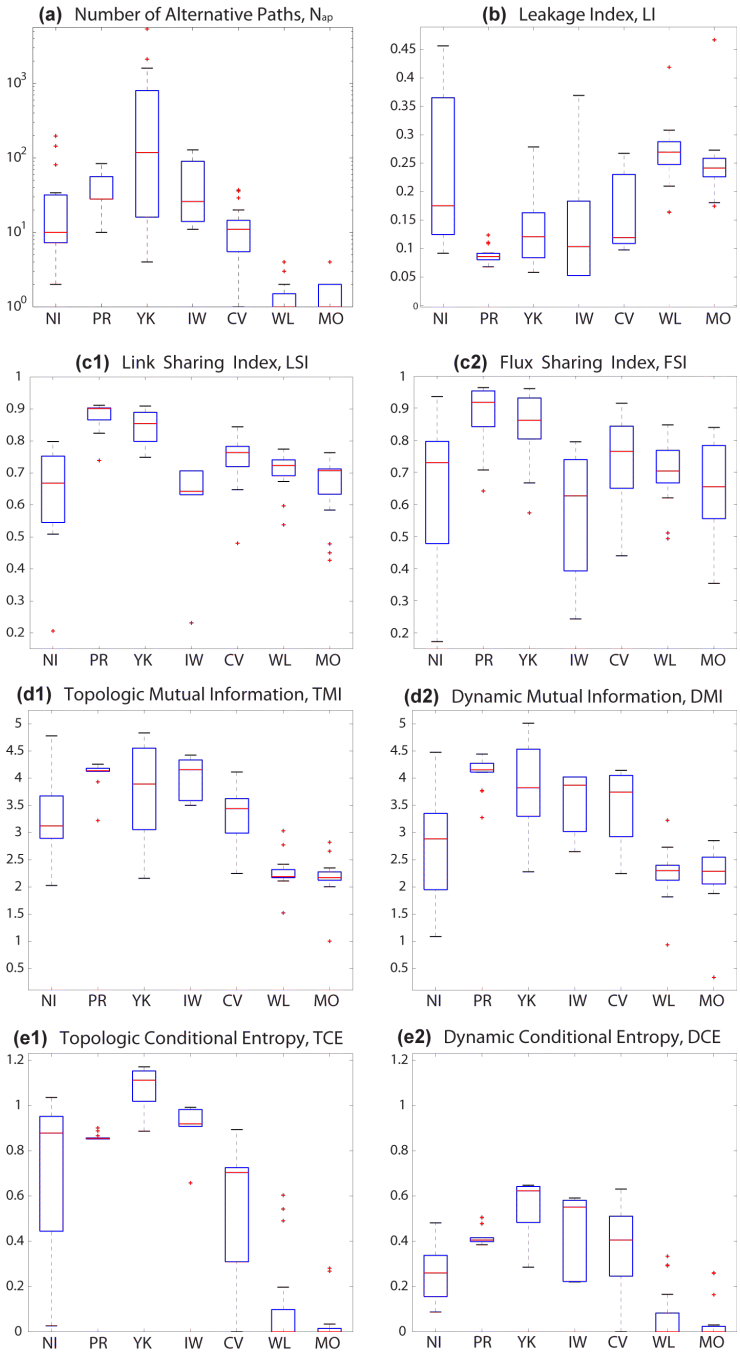

Figure 5. Summary of topologic (a, c1-e1) and dynamic (b, c2-e2) complexity metrics for the seven deltas (NI = Niger, PR = Parana, YK = Yukon, IW = Irrawaddy, CV = Colville, WL = Wax Lake, MO = Mossy). We note that for a binary tree (for depth d =10) the topologic metrics are equal to: N_{ap} =1, LSI = 0.80, TMI =1.99 and TCE =0 and the Wax Lake and Mossy deltas are the closest to those values, as expected.

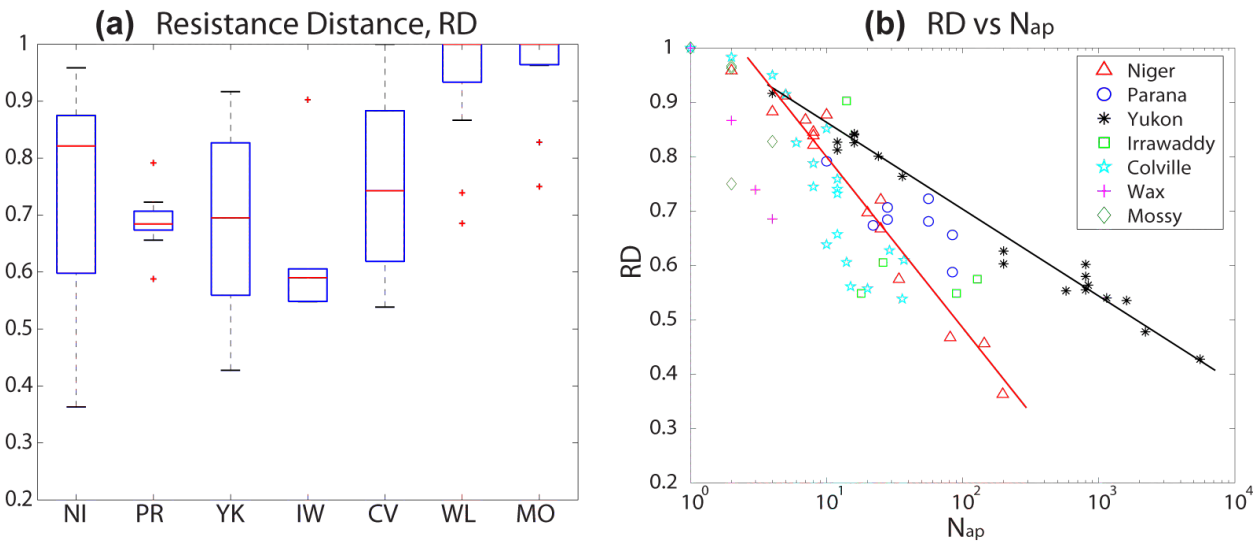

Figure 6. Resistance Distance. (a) Resistance Distance for each delta, and (b). Resistance Distance vs. Number of alternative paths. Note that the two metrics relate to each other as expected (the larger the Number of alternative paths the smaller the Resistance Distance, e.g., a clear relationship in Niger and Yukon deltas) but this relationship is non-trivial for some deltas depicting pronounced differences (e.g., different slopes). For a binary tree, the Resistance Distance is equal to 1 and the Number of alternative paths is also 1 for all subnetworks. (Note: NI = Niger, PR = Parana, YK = Yukon, IW = Irrawaddy, CV = Colville, WL = Wax Lake, MO = Mossy)

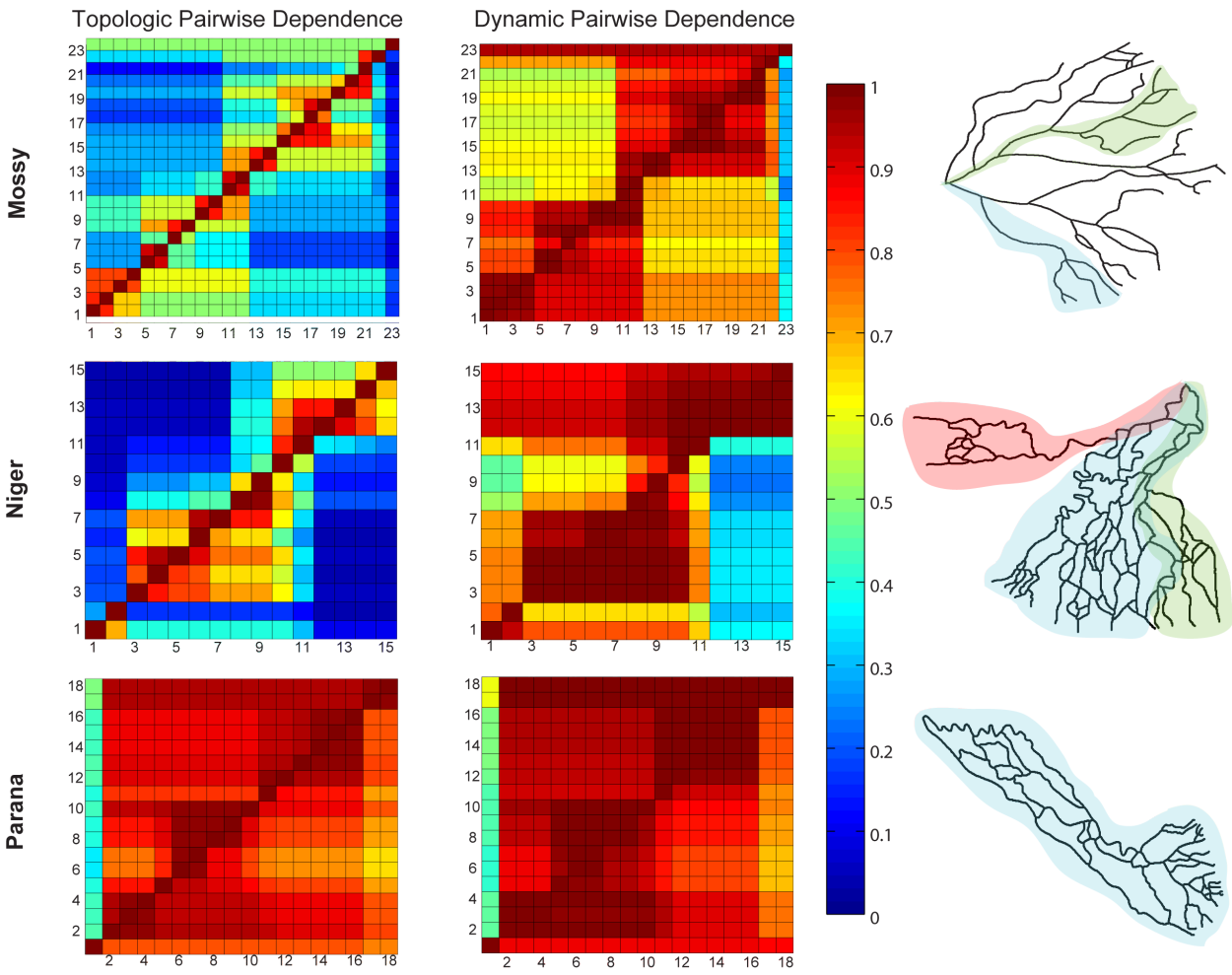

Figure 7. Subnetwork to Subnetwork Topologic (left panels) and Dynamic (center panels) Pairwise Dependence. Outlets are indexed consecutively and counterclockwise starting with the leftmost one where the delta is plotted with the apex on the figure's top and outlets at the bottom. The cell (i,j) of the topologic (dynamic) dependence represents the percentage of links (fluxes) shared by subnetworks i and j with respect to the total number of links (fluxes) in subnetwork i. Red (blue) colors represent high (low) values of sharing. Right panels illustrate the topologic and dynamic units at intermediate scales that arise from the interpretation of the pairwise dependence.

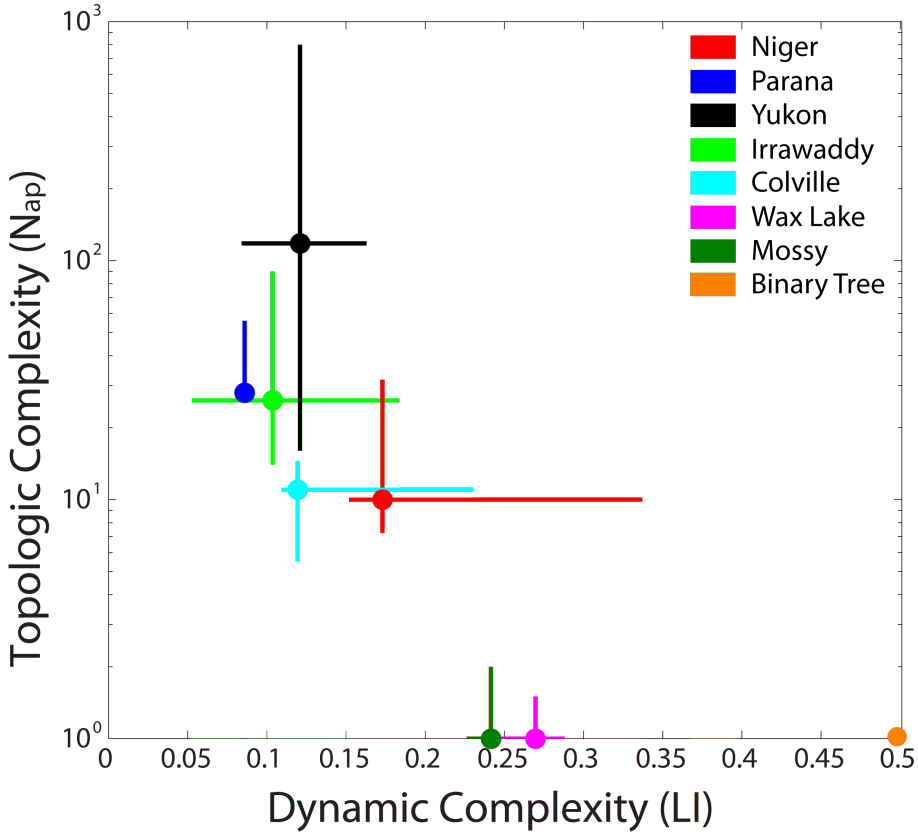

Figure 8. Topo-dynamic Complexity Space for deltas. We define a 2D space where the x-axis corresponds to the dynamic exchange of the different subnetworks measured by the Leakage Index, and the y-axis corresponds to the topologic complexity measured by the Number of alternative paths from apex to outlet. Each colored cross corresponds to a different delta, and the orange dot corresponds to a binary tree. The vertical (horizontal) component of each cross runs from the 25th until the 75th percentile of the Number of alternative paths (Leakage Index). The filled dot for each delta corresponds to the intersection point of the medians of both parameters: Number of alternative paths and Leakage Index.

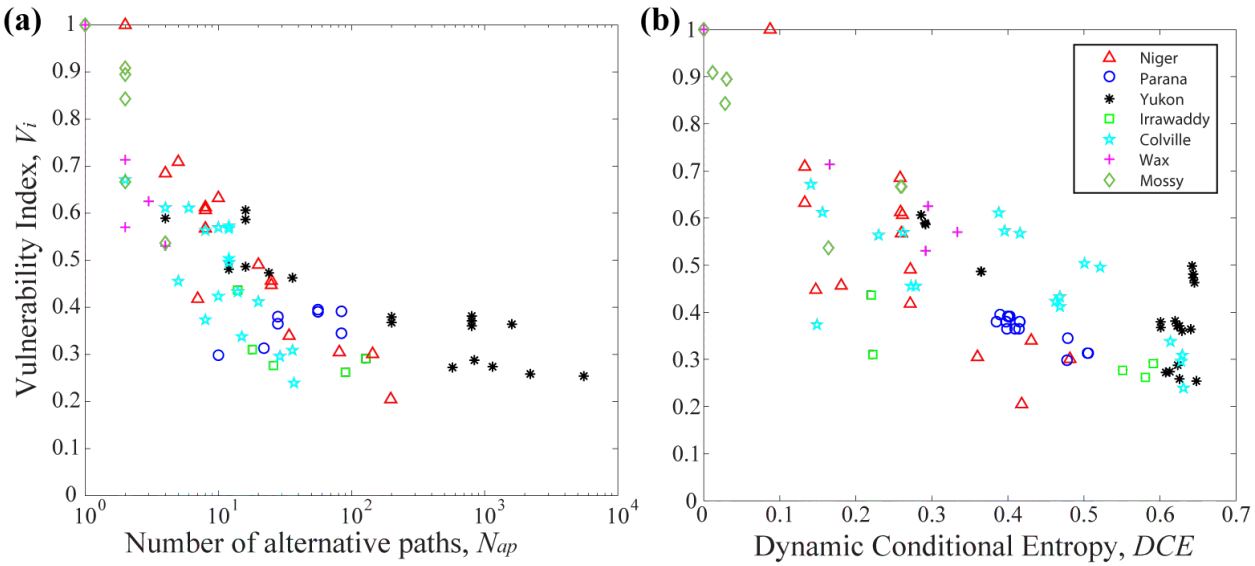

Figure 9. Relation of Vulnerability to Topologic and Dynamic Complexity. Vulnerability Index vs. Number of alternative paths (left) and vs. Dynamic Conditional Entropy (right). As expected, the more complex a delta is the more "robust" it is to change. This is because alternative paths and equitable flux distribution minimize the effects of a flux change in upstream links to the flux reaching the outlet.

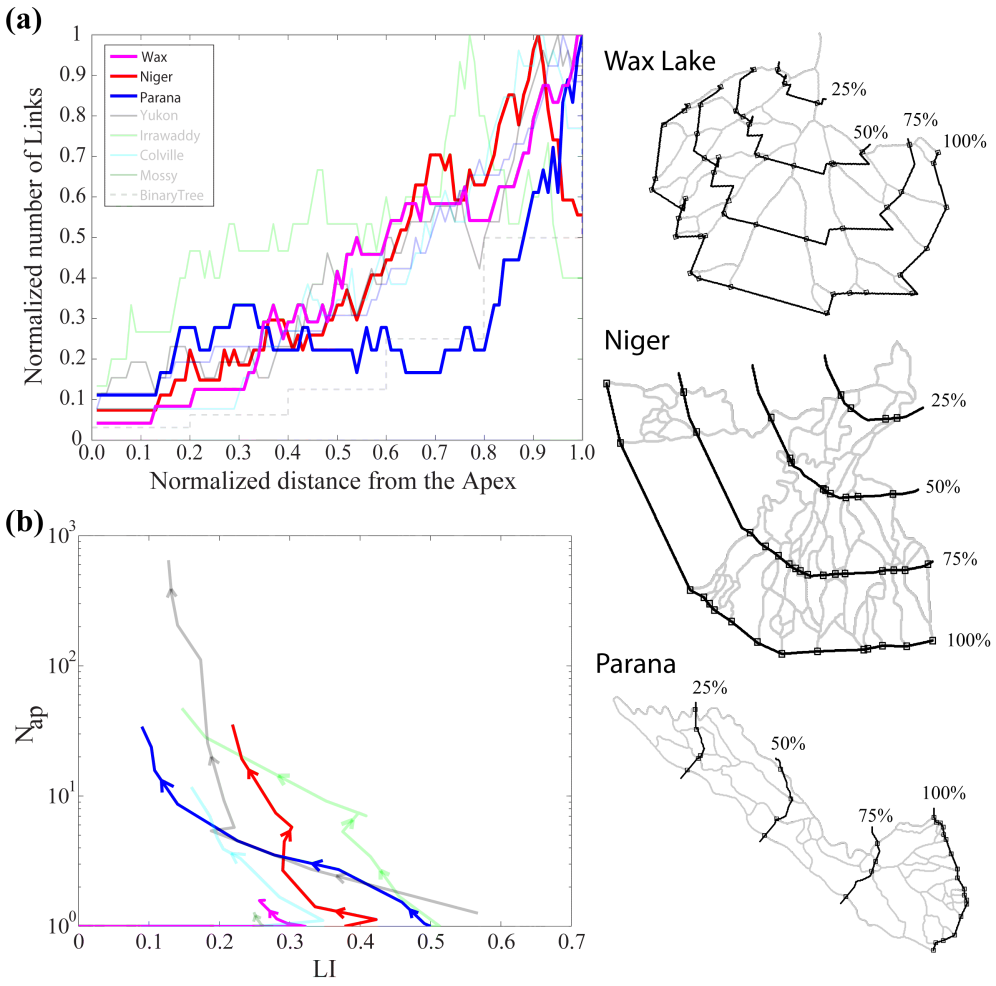

Figure 10. Spatially explicit metrics of complexity. (Right panels) Schematic representation of contours radially scaled at normalized distances of 25%, 50%, 75% and 100% of the current shoreline. The squares show the intersections at the different distances. (a) *Delta width function* for the seven deltas examined. (b) Each line represents the smoothened trajectory in the topo-dynamic complexity space (intersection of the mean of both Leakage Index and Number of alternative paths) for each radially scaled delta from the apex to the shoreline. Note, that if actual data on shoreline and channel network evolution existed this plot would capture the progression of the topo-dynamic complexity of the evolving delta.

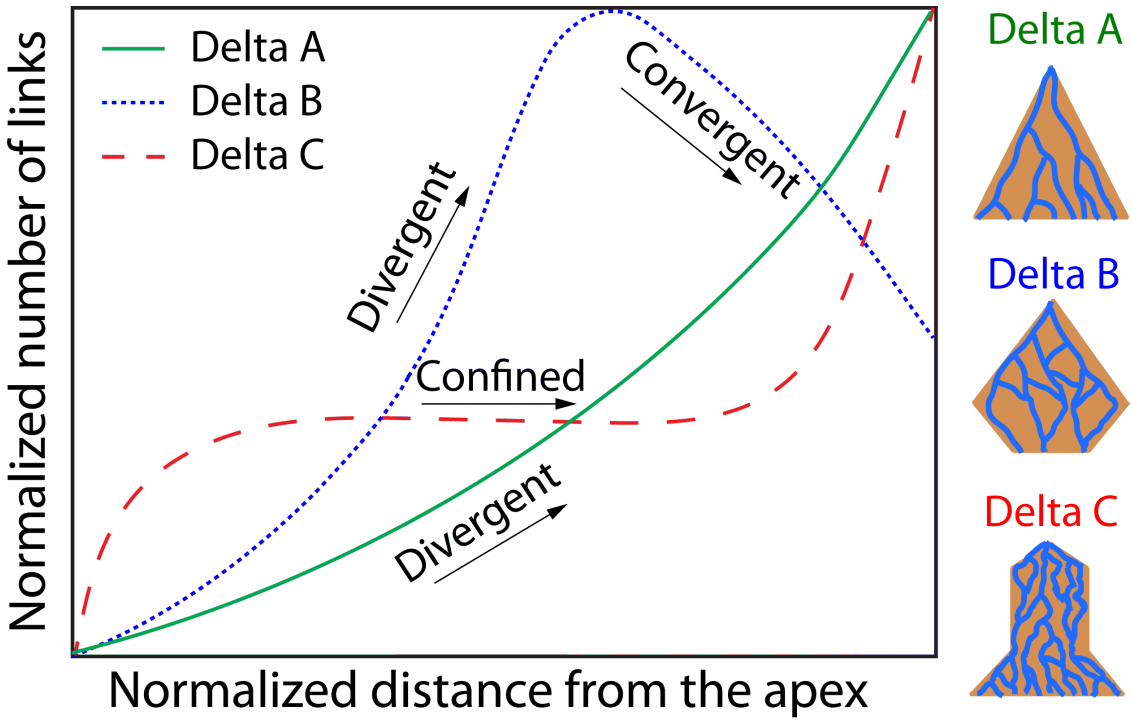

Figure 11. Width function and delta network shape. Different trends can be observed in the delta width function (normalized number of intersected links vs. normalized distance from apex): (i) *Divergent*, illustrated by Delta A, for which the delta width function is an increasing function of the distance from the apex, (ii) *Convergent*, illustrated in the lower portion of Delta B wherein the delta width function is a decreasing function of the distance from the apex, and (iii) *Confined*, illustrated by the middle portion of Delta C, for which the delta width function remains constant as the distance from the apex increases.

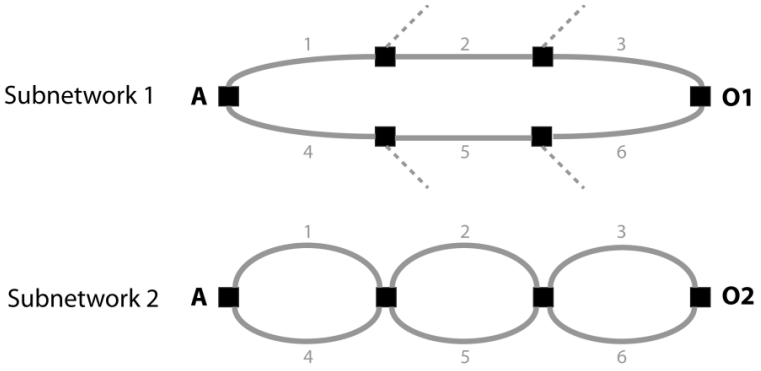

Figure A1. Illustration of two subnetworks. Subnetwork 1: Apex connects to the outlet 1 (O1) via two paths, each composed of three links (note that the presence of vertices in the path implies for a delta system that other links (dashed lines) initiate at each of those vertices but drain to another outlet). Subnetwork 2: Apex drains to the outlet 2 (O2) via a more intricate structure.